ChemComm

ROYAL SOCIETY OF CHEMISTRY

FEATURE ARTICLE

View Article Online
View Journal | View Issue

Cite this: *Chem. Commun.*, 2023, 59, 6314

Emerging covalent triazine framework-based nanomaterials for electrochemical energy storage and conversion

Yong Zheng, *[a] Niaz Ali Khan,[b] Xuepeng Ni,[a] Kai A. I. Zhang, *[c] Yi Shen,[d] Niu Huang,[a] Xin Ying Kong[e] and Liqun Ye *[a]

Received 15th February 2023,
Accepted 19th April 2023

DOI: 10.1039/d3cc00712j

rsc.li/chemcomm

Recently, the increasing concerns regarding environmental and energy-related issues due to the use of fossil fuels have triggered extensive research on sustainable electrochemical energy storage and conversion (EESC). In this case, covalent triazine frameworks (CTFs) possess a large surface area, tailorable conjugated structures, electron donating–accepting/conducting moieties, and excellent chemical and thermal stabilities. These merits make them leading candidates for EESC. However, their poor electrical conductivity impedes electron and ion conduction, leading to unsatisfactory electrochemical performances, which limit their commercial applications. Thus, to overcome these challenges, CTF-based nanocomposites and their derivatives such as heteroatom-doped porous carbons, which inherit most of the merits of pristine CTFs, lead to excellent performances in the field of EESC. In this review, initially, we briefly highlight the existing strategies for the synthesis of CTFs with application-targeted properties. Next, we review the contemporary progress of CTFs and their derivatives related to electrochemical energy storage (supercapacitors, alkali-ion batteries, lithium–sulfur batteries, *etc.*) and conversion (oxygen reduction/evolution reaction, hydrogen evolution reaction, carbon dioxide reduction reaction, *etc.*). Finally, we discuss perspectives on current challenges and recommendations for the further development of CTF-based nanomaterials in burgeoning EESC research.

1. Introduction

Advanced and renewable energy conversion and storage technologies such as rechargeable electrochemical batteries, supercapacitors and electrochemical water splitting devices play pivotal roles in the existing energy systems, which aim to urgently address the energy crisis and environment pollution.[1–4] Therefore, numerous studies have been reported on the development of sustainable energy-related techniques since the commercialization of lithium-ion batteries (LIBs) in the 1990s.[5] However, given that the cycle/rate performance, energy/power density, safety and fabrication cost of these energy-related devices need further improvement, exploring new materials for novel electrochemical EESC systems to realize enhanced performances and lower costs is necessary but highly challenging.[6]

To date, various nanomaterials have been exploited in this emerging field, including metal-based (*e.g.*, Pt, Ir, Co, Fe, Mn and Cu) nanomaterials and their nanocomposites (alloys, carbides, nitrides, sulfides, *etc.*), metal-free nanocarbons, and porous covalent organic polymers (COPs).[7] For their utilization as favourable electrode materials in the promising EESC devices, the following characteristics are primarily required: (1) high conductivity to ensure efficient electron and ion transfer, (2) appropriate pore structure and distribution to guarantee the adequate exposure of high-density active sites and excellent mass transport, and (3) great chemical and thermal stability to support the desirable long-term stability and recyclability. In this regard, porous COPs have been considered as one of the most promising materials for a decade owning to their feasible physical and chemical properties, porous structures, and high stability. Among them, covalent triazine frameworks (CTFs) are triazine-containing and nitrogen (N)-rich porous organic frameworks, which were first

[a] *College of Materials and Chemical Engineering, Key Laboratory of Inorganic Nonmetallic Crystalline and Energy Conversion Materials, China Three Gorges University, Yichang 443002, P. R. China. E-mail: zhengyong@ctgu.edu.cn, lqye@ctgu.edu.cn*
[b] *Key Laboratory of Textile Fiber and Products (Wuhan Textile University), Ministry of Education, Wuhan, 430200, P. R. China*
[c] *Department of Materials Science, Fudan University, Shanghai 200433, P. R. China. E-mail: kai_zhang@fudan.edu.cn*
[d] *College of Environment, Zhejiang University of Technology, Hangzhou, 310032, P. R. China*
[e] *School of Chemistry, Chemical Engineering and Biotechnology, Nanyang Technological University, 21 Nanyang Link, Singapore*

reported in 2008 (through the trimerization of aromatic nitriles).[8] Since then, CTFs have attracted wide attention due to their attractive properties (Fig. 1).[9–11] Owing to the highly stable triazine units of CTFs, they possess high chemical and thermal stability. Compared with most conventional metal-containing materials, CTF-based candidates also display great tunability owing to their rich surface chemistries. Moreover, their porous nature enhances the mass diffusion including active intermediates, reactants, and products, which is beneficial for electrochemical reactions.[12] Besides, CTFs can be easily synthesized using relatively inexpensive monomers in high yields, thereby reducing the manufacturing costs for large-scale fabrication.[13] Furthermore, the appropriate choice of monomer with different chemical structures and components can produce CTFs with a variety of desirable moieties, large specific surface areas (SSA),[14] abundant heteroatom active sites, and tunable porosities for applications in the burgeoning field of EESC.[15]

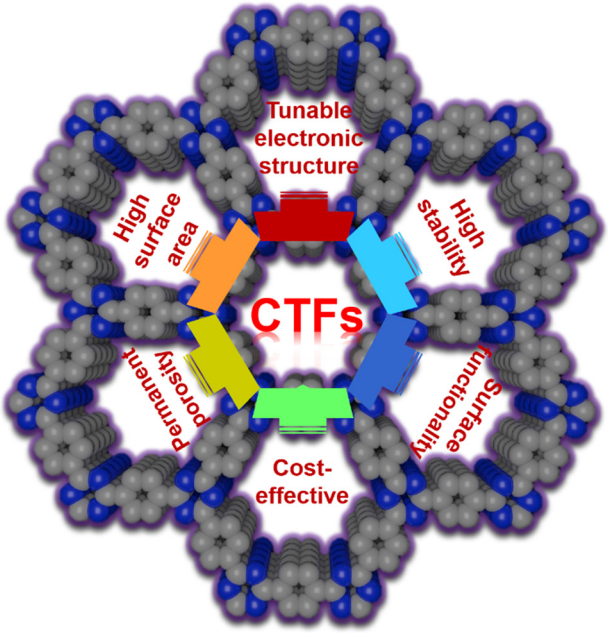

Fig. 1 Chemical structures and promising properties of CTFs.

The presence of heteroatoms in a structural unit can serve as redox active sites for various electrochemical reactions to occur. Most pristine CTFs are semiconductors or insulators, but the introduction of conjugated molecules in their framework or doping with conductive components can significantly improve their conductivity,[16] ensuring their application in EESC systems. Furthermore, the unique structure of CTFs,

Yong Zheng

Yong Zheng is an Assistant Professor at the College of Materials and Chemical Engineering, China Three Gorges University (CTGU). He received his PhD in 2021 from the College of Materials Science and Engineering at Donghua University. He joined Fudan University for a cooperative project research in the Department of Materials Science (2019–2021). His current research interests focus on the micro/nano structure design of covalent organic polymer-based materials and their application in photo/electrocatalysis.

Kai A. I. Zhang

Kai Zhang did his PhD at the University of Cologne, Germany and partly at the University of Strathclyde, Glasgow, UK. After working as a Postdoctoral Researcher with Prof. Markus Antonietti at the Max Planck Institute of Colloids and Interfaces, Potsdam, Germany, he joined the Max Planck Institute for Polymer Research in 2013 as an independent research group leader in the Department of Physical Chemistry of Polymers under Prof. Katharina Landfester. In 2019, he was appointed to Full Professor by the Department of Materials Science at Fudan University, Shanghai, China. His research interests include the development of organic porous materials, macromolecular photocatalysts and their applications in organic photo-redox reactions, energy-related catalysis, fine chemistry, photo-biocatalysis, etc.

Liqun Ye

Liqun Ye obtained his BS Degree from Qiqihar University, PR China, in 2008, and his PhD from Wuhan University, PR China, in 2013, under the supervision of Prof. Ling Zan. Subsequently, he worked in Prof. Po Keung Wong's group as a Research Assistant at the Chinese University of Hong Kong (2015–2016). At present, he works at China Three Gorges University. His current research focuses on the synthesis of functional materials and their applications in the fields of environment remediation and new energy production.

which possess well-ordered micro/mesoporous channels and a plethora of heteroatom-containing organic linkers, makes them one of the most alluring candidates as precursors for a variety of heteroatom-doped porous nanocarbons with various morphologies, excellent conductivity, and large SSA under suitable pyrolysis conditions.[17,18] Besides an enhancement in conductivity, CTF-derived nanocarbons can also subsequently inherit the aforementioned merits of their CTF precursors, making them suitable for multifarious electrochemical applications.[19–22]

The application of CTFs in gas adsorption/storage[23–40] and catalysis in relation to the energy and environment issues[41–44] has been well-reviewed previously. However, in recent years, many important breakthroughs have been reported for CTF-based nanomaterials in the field of EESC, which have not been comprehensively summarized. Hence, a comprehensive review concerning the latest progress of pristine CTFs, CTF-based nanocomposites, and their derived nanomaterials in EESC systems is urgently needed. In this contribution, we focus on the current state-of-the-art synthesis of CTFs and their applications in the emerging field of EESC. Also, we underscore some fundamental attempts toward a better understanding of the design principles for the development of novel CTF-based nanomaterials for boosted electrochemical performances. The existing challenges and further opportunities in this exciting field are also included.

2. CTF synthesis methods

Since Thomas *et al.* proposed the term CTF and first synthesized it *via* the ionothermal approach using nitrile monomers in 2008,[8] the techniques for the synthesis of CTFs have made great progress and developed vigorously over the past decade.[12] Various synthesis methods have been discovered to meet the practical applicability of CTFs. Although most of the existing methods focus on the direct or indirect cyclo-trimerization of nitrile groups, other pathways such as Friedel–Crafts reactions, aromatic nucleophilic substitution reactions, and C–C coupling routes can also be used for the synthesis of CTFs.

2.1 Ionothermal synthesis

CTF-1 was first reported using a $ZnCl_2$-ionothermal synthetic route by Thomas *et al.*[8] It involves the use of 1,4-dicyanobenzene as a single building unit, whereas melted $ZnCl_2$ salt serves as both the solvent and catalyst. Through gradual self-trimerization of intermolecular cyano groups, CTF-1 was obtained. Since then, a myriad of CTFs has been synthesized using this method and various cyano-containing monomers (Fig. 2a).[45–50] The as-prepared CTFs not only possess a high N content, but also exhibit great chemical and thermal stability even in harsh environments. In 2010, Qiu *et al.* further optimized the reaction conditions, in which a microwave-enhanced ionothermal method was introduced.[51] Compared with the traditional ionothermal method, the microwave method can greatly reduce the time and energy needed to synthesize CTFs.

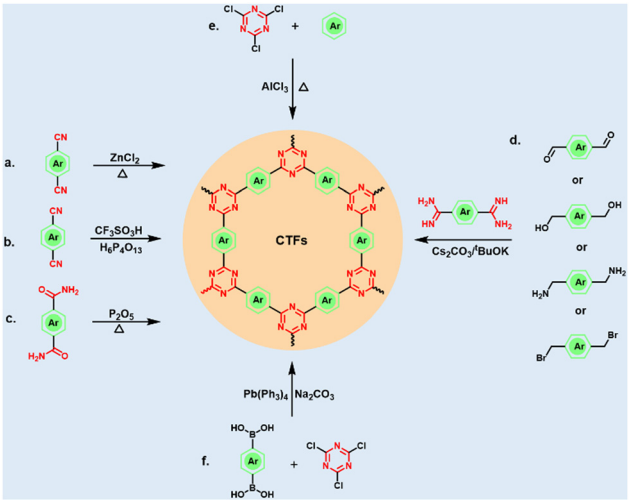

Fig. 2 Synthetic reactions and routes for the preparation of CTFs, including ionothermal method, superacid-catalyzed trimerization, P_2O_5-catalyzed method, strong base-catalyzed polycondensation, Friedel–Crafts reactions and C–C coupling reactions.

However, owing to the severe reaction conditions, complex operation, and the poor crystallinity of the CTF products, the further application of the ionothermal synthesis strategy is greatly restricted. In addition, under the condition of high ionothermal temperature, aromatic compounds and heterocyclic aromatic compounds are unavoidably carbonized. Alternatively, Wang *et al.* reported an ionothermal method for the synthesis of CTFs using a triplex mixture containing NaCl–KCl–$ZnCl_2$ salts with an approximate melting point of 200 °C.[52] The relatively low-temperature condition facilitated the polycondensation process, while practically circumventing the carbonization of the polymeric networks.

2.2 Superacid-catalyzed synthesis

Early in 1941, Cook *et al.* employed chlorosulfonic acid to synthesize triazine-based materials *via* the trimerization of aromatic nitriles.[53] In 2012, Cooper *et al.* catalyzed this trimerization reaction using trifluoromethanesulfonic acid (CF_3SO_3H) at both room temperature and under microwave condition (Fig. 2b).[54] This was also the beginning of the synthesis of CTFs catalyzed by strong acids. Subsequently, Dai *et al.* first reported the CF_3SO_3H-catalyzed synthesis of CTF membranes with fluorescence characteristics.[55] In addition, they also reported a simple but efficient superacid-catalyzed transformation towards the synthesis of highly crystalline CTFs. In a separate study, Thomas *et al.* synthesized a CTF with trifluoromethylsulfonic acid and chloroform as the catalyst and solvent, respectively.[56] Alternatively, Wang *et al.* synthesized DA-CTF catalyzed by CF_3SO_3H with a unique electronic structure and porosities.[57] In addition, Zhao *et al.* successfully synthesized CTF using *p*-toluenesulfonic acid as a catalyst.[58] After that, Dai *et al.* utilized CF_3SO_3H as an acid catalyst to form AB stacking CTF-1 firstly, and then a mechanochemistry-driven approach was employed to achieve crystalline CTFs assisted by

alkaline molten salts.[59] Separately, Xu *et al.* developed another $H_6P_4O_{13}$-catalytic strategy to synthesize CTFs at a relatively high temperature (400 °C).[60] The developed CTFs exhibited ideal ordered structures, pore distribution, and large SSA. Importantly, they also managed to produce highly crystalline CTFs on the kilogram-scale. Compared with the high-temperature ionothermal synthesis, superacid catalysis synthesis under relatively mild conditions can effectively avoid carbonization of the porous framework, resulting in higher crystallinity of the CTFs. However, the high corrosivity and cost of superacid limit the scalable application of this approach.

2.3 Phosphorus pentoxide (P_2O_5)-catalyzed synthesis

In 2018, Baek *et al.* employed P_2O_5 as a catalyst to synthesize pCTF-1 directly from aromatic amide instead of aromatic nitrile *via* the condensation reaction (Fig. 2c).[61] According to powder X-ray diffraction, pCTF-1 was highly crystallized and possessed a large SSA of 2034.1 $m^2\ g^{-1}$. Later, they converted both biphenyl-based amide and nitrile monomers to CTFs using P_2O_5 as the catalyst.[62] Interestingly, the direct conversion of amide monomers resulted in the formation of pCTF with high crystallinity and well-ordered pores together with large SSA. Since then, a series of CTFs has been constructed using the P_2O_5-catalyzed method.[63] This approach is highly environmental-friendly compared to the classical synthesis of CTFs catalyzed by Lewis acids or superacid catalysts. This novel approach for the fabrication of CTFs serves as a promising platform for the formation of satisfactory framework structures towards their practical application in the field of EESC.

2.4 Low-temperature polycondensation synthesis

Alternatively, Tan *et al.* first fabricated CTFs using aldehydes and amidines as building modules (Fig. 2d).[64] This method not only overcomes the drawback of carbonization by the ionothermal method, but also avoids the corrosiveness associated with superacid. These results provide a novel strategy for the design and synthesis of functional earth-abundant CTFs for energy storage applications. Soon after, they used cesium carbonate (Cs_2CO_3) to control the oxidation of alcohol hydroxyls to aldehydes, which then reacted with amidines to form CTF-HUSTs (Fig. 3a).[65] The as-prepared CTF exhibited high crystallinity and a large SSA of 599 $m^2\ g^{-1}$ (Fig. 3b). This method is relatively simple and it can be carried out in an open system, which serves as a promising method for industrial applications. Moreover, the CTFs synthesized by this method have higher thermal stability and crystallinity. This is a significant breakthrough in the synthesis of crystalline CTFs.

2.5 Other synthesis methods

Besides the above-mentioned methods, CTFs can also be prepared through direct coupling methods using triazine moieties connected with other aromatic monomers. The pre-existence of a triazine core avoids the utilization of harsh reaction conditions (high temperature, superacid, strong base, *etc.*). Moreover, this strategy can yield CTFs with modular characteristics, which is helpful to disclose the influence of their

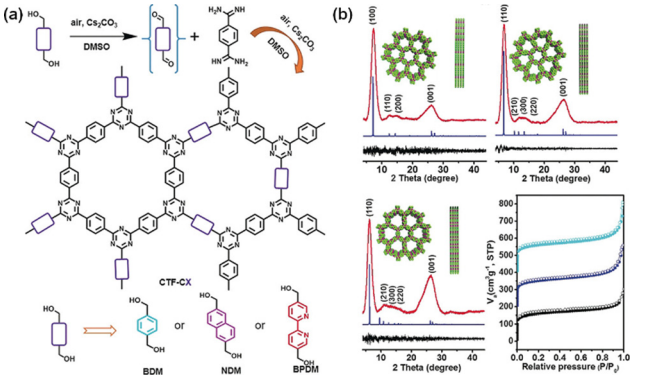

Fig. 3 (a) Pathways for the synthesis of the crystalline CTFs. (b) XRD patterns and N_2 adsorption and desorption isotherms of crystalline CTFs. Reproduced from ref. 65 with permission from Wiley-VCH, Copyright 2018.

chemical composition on their performance in electrochemical applications.[66] Recently, cyanuric chloride and various aromatic compounds were converted into various types of CTFs employing $AlCl_3$-catalyzed Friedel–Crafts reaction (Fig. 2e).[67–70] This methodology is straightforward, cheap, and more atom-efficient in comparison to other pathways. The obtained CTFs also possess high thermo-chemical stability in a variety of aqueous and organic solvents. Borchardt *et al.* reported the scaled-up synthesis of CTFs *via* a solvent-free mechanochemical Friedel–Crafts method.[71] In addition, some CTFs have also been prepared through Ni-catalyzed Yamamoto coupling,[72] Pd-based Sonogashira coupling,[73] aromatic nucleophilic substitution reactions,[74] Mannich reactions,[75] *etc.* For example, Wang *et al.* designed three CTFs using palladium-catalysed Suzuki cross-coupling polycondensation reaction (Fig. 4).[76] These approaches provide better control of the chemical structures and surface functionality of CTFs, which are suitable for various catalytic applications. However, the resulting CTFs are almost amorphous owing to the kinetically controlled manner of these reactions.

Table 1 summarizes the different classes of synthesis methods that are currently available. It is worth noting that each approach has its own advantages and disadvantages, and there is no one-size-fits-all strategy. Therefore, it can be challenging to

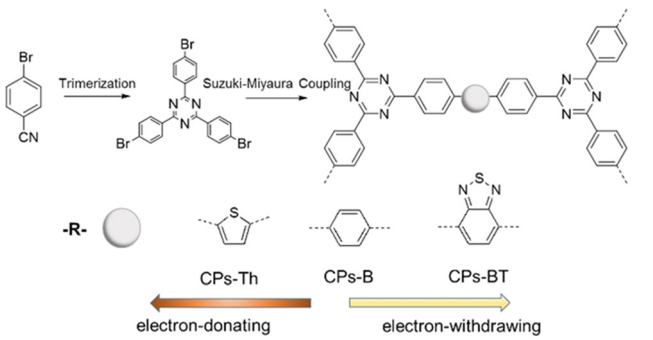

Fig. 4 Synthesis of CTFs by Suzuki cross-coupling. Reproduced from ref. 76 with permission from Elsevier, Copyright 2018.

Table 1 A comparison of different synthesis methods and the corresponding features of CTFs

Synthesis method	Reaction condition	Crystallinity	Specific surface area ($m^2\ g^{-1}$)	Decomposition temperature (°C)	Structural integrity	Ref.
$ZnCl_2$-ionothermal	Harsh	Moderate	2475	~360	Partial carbonization	8
NaCl–KCl–$ZnCl_2$-ionothermal	Moderate	Moderate	—	—	Good	52
CF_3SO_3H-catalyzed	Moderate	Amorphous	1152	~250	Moderate	54
P_2O_5-catalyzed	Harsh	Good	2034.1	~400	Moderate	61
Polycondensation	Mild	Good	—	~210	Good	64
Friedel–Crafts	Mild	Amorphous	590	~500	Good	71

select a suitable synthesis method for attaining the target CTFs. For instance, high-temperature ionothermal synthesis methods lead to partial carbonization of the obtained CTF materials. Alternatively, the involvement of high-cost and corrosive superacid catalysts limits their large-scale production for practical application. Considering their industrialization prospect, the primary concerns are the actual application and production costs rather than the CTFs themselves. Therefore, the further development of functional CTF materials based on low operational cost, while rendering satisfactory crystallinity is highly desirable, but challenging.

3. Electrochemical energy storage and conversion applications

The high thermo-chemical stability coupled with the large SSA and high N content of CTFs make them alluring materials for various practical applications. The majority of CTFs are reported to be porous materials for gas storage/capture towards hydrogen,[33,39] carbon dioxide,[26,32,77] and methane.[78] Importantly, the basic N sites in CTFs can act as excellent catalytic sites, which has been demonstrated in the field of EESC devices.[79]

3.1 Electrochemical energy storage

3.1.1 Supercapacitors. Supercapacitors (SCs) or ultracapacitors, also referred to electrochemical capacitors (ECs), are extensively explored in terms of their high power densities, rapid charging–discharging rates, and long-cycle lifespans.[80] SCs are mainly classified into two types based on their energy storage mechanism, as follows: (i) electrochemical double layer capacitor (EDLC), where the capacitance results from the electrostatic charge accumulated at the electrode and electrolyte interface, and (ii) pseudocapacitor, which is based on a rapid and reversible faradaic process.[81] In EDLCs, the accessible surface area of the electrode material to electrolyte ions plays a key role in the electrochemical performances. Therefore, porous carbon materials of various types, namely, activated, templated, carbide-derived, graphene, and nanotubes, are generally used as the electrode material due to their large SSA, good thermo-chemical stability, and electrical conductivity.[82] In the case of pseudocapacitors, noble or inexpensive transition metal oxides or hydroxides, heteroatom-containing porous polymers, conducting polymers, and carbon materials with O or N-containing functional groups on their surface are commonly employed as the electro-active materials. The performance of pseudocapacitors mainly relies on the site density (SD, sites $g_{catalyst}^{-1}$) of the redox-active species and the exposed surface area of the electrode materials. In summary, a perfect electrode material should exhibit the characteristics of high conductivity, large SSA, fast ion mobility, and excellent hydrophilic wettability.

It is well-known that the energy density of SCs is comparatively lower than that of batteries. The improvement in the energy density of SCs has been achieved by introducing heteroatoms (including N, O, P, and S) in the matrix of electrode materials.[83] Among them, the incorporation of N atoms has attracted significant research attention due to their ability to enhance the wettability and enlarge the accessible electro-active surface area, thereby endowing the electrodes with pseudo-capacitance to further enhance their capacitive performance.[84] Pristine CTFs with adjustable pore sizes, heteroatom-doped organic skeleton and copious redox-active species possess great potential to serve as electrode materials for SCs given that they possess pseudo-capacitance properties. Moreover, the large SSA of CTFs increases the electrode/electrolyte contact interfaces, thereby enhancing their electrochemical efficiency when used as electrodes in EDLCs.

Zhi *et al.*[85] prepared CTF-1 amorphous analogues of terephthalonitrile-based N-rich networks, which were denoted as TNNs. TNNs were employed as electrode materials for SCs, exhibiting a specific capacitance of 298 F g^{-1} at 0.2 A g^{-1}. In a subsequent study, they reported a series of N-containing microporous CTFs featuring designable and controllable N-doped electro-active sites. As an electrode, the best sample demonstrated a high energy density and power density of 62.7 W h kg^{-1} and 8750 W kg^{-1} based on high-voltage ionic liquid-based electrolytes, respectively.[86] Deng *et al.* reported the synthesis of conductive microporous CTFs based on tetracyanoquinodimethane (TCNQ-CTFs)-containing a high N quantity (>8%) and large SSA (>3600 $m^2\ g^{-1}$).[87] The authors observed an ultra-high specific capacitance for these CTFs with a value of over 380 F g^{-1}, high energy density of 42.8 W h kg^{-1}, and outstanding cycling stability up to 1000 cycles without any noticeable degradation in capacitance. Subsequently, Yang *et al.*[88] prepared a crystalline CTF through a simple condensation reaction without any catalysts. In this study, the electrode demonstrated a high specific capacitance of 130.5 F g^{-1} at a current density of 2 A g^{-1} with 28.5% decrease after 4500 galvanostatic charge/discharge (GCD) cycles. In another study, Kuo *et al.*[89] synthesized pyrene-containing CTFs (pyrene-CTF-10 and pyrene-CTF-20), which exhibited ultrahigh

specific capacitances at a current density of 0.5 A g^{-1} (380 F g^{-1} and 500 F g^{-1} for pyrene-CTF-10 and pyrene-CTF-20 in 1 M KOH electrolyte, respectively). Interestingly, the obtained CTFs retained ≈97% of their original capacitance after 2000 cycles. Similarly, this group[90] reported that a two-dimensional (2D) hexagonally ordered CTF showed excellent electrochemical properties owing to its conjugated nature decorated with redox-active groups. It exhibited the highest specific capacitance of 51.3 F g^{-1} at 0.2 A g^{-1}. Besides, they also synthesized a series of bicarbazole-based CTFs (Car-CTFs) under ionothermal conditions.[32] The Car-CTF series exhibited the optimal capacitance of 545 F g^{-1} at 5 mV s^{-1}, and also showed a remarkable coulombic efficiency of 96.1% after 8000 cycles. Besides, this group[91] also reported the synthesis of a hollow microtubular CTF using a template-free [3+2] reaction. The obtained CTFs were characterized with extremely high crystallinity together with a large SSA (*ca.* 1855 m^2 g^{-1}) and ultrahigh thermal stability. In addition, the authors observed an excellent supercapacitor performance with a capacitance of close to 256 F g^{-1} at a current density of 0.5 A g^{-1}, together with promising cycling stability (98.8% capacitance retention after 1850 cycles) and a high energy density of 43 W h kg^{-1}.

Furthermore, the hydrophilic nature of certain CTFs and their functional pores serve as the active sites for ion adsorption. In this regard, Ning *et al.*[92] prepared p-CTF and it was used as an electrode, which showed excellent capacitive behavior, with the highest specific capacitance value of 122.63 F g^{-1} under a scan rate of 1 mV s^{-1} in aqueous 1 M NaCl solution. Yang *et al.* synthesized redox-active CTF materials by reacting 1,4-piperazine dicarboxaldehyde (PDC) and melamine (MA) as building units *via* a Schiff-base condensation.[93] The prepared CTFs exhibited the highest specific capacitance of 335 F g^{-1} and 94 F g^{-1} in a two-electrode system and three-electrode system at a current density of 1.0 A g^{-1}, respectively. Similarly, Bhaumik *et al.*[94] reported a novel CTF (termed TDFP-1) *via* the solvothermal condensation reaction between 1,3,5-tris-(4-aminophenyl)triazine and 2,6-diformyl-4-methylphenol. TDFP-1 performed excellently in energy storage applications, which exhibited a maximum specific capacitance of 354 F g^{-1} (scan rate of 2 mV s^{-1}) and a remarkable 95% retention even after 1000 cycles at 10 A g^{-1} due to its intrinsic microporosity and large SSA.

Recently, Kaskel *et al.*[95] prepared a novel CTF based on pyridine units by controlling the reaction temperature. They applied pyridine-based CTFs as symmetrical SCs and observed a specific capacitance of 141 F g^{-1}. The residual $ZnCl_2$ could be dissolved in water to obtain an aqueous electrolyte. Particularly, halogens as unique heteroatoms have also been incorporated in CTFs to improve their capacitance. Similarly, Wang *et al.*[96] observed that a fluorinated CTF (FCTF) showed an excellent capacitance of 379 F g^{-1} at 1 A g^{-1}, an impressive reusability of 96.8% together with high coulombic efficiency of 99.6% at 5 A g^{-1} after 10 000 cycles. These findings demonstrate that halogen-functionalized CTFs can serve as potential electrode materials for the development of high-performance SCs. Oh *et al.* designed an electronically conjugated nanoporous CTF and employed it as an electrode material, which acquired a stable energy density value of 147.5 W h kg^{-1} in solid-state

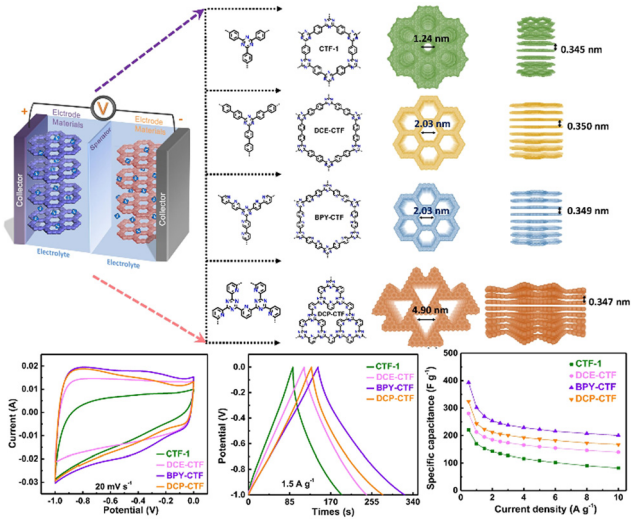

Fig. 5 Schematic diagram of SC configuration, design, and synthesis, together with the SC performance of CTF-1, DCE-CTF, BPY-CTF, and DCP-CTF. Reproduced from ref. 98 with permission from Elsevier, Copyright 2022.

flexible supercapacitors.[97] This work further diversified the roles of CTFs in flexible and portable devices such as smart wearable electronic devices, and auto-electric vehicles. Besides, as shown in Fig. 5, Qiao *et al.* studied the role of the porous environment and N content in CTFs in SCs.[98] They observed a specific capacitance of 393.6 F g^{-1} at 0.5 A g^{-1} for BPY-CTF, which was attributed to the synergistic effects of the suitable pore channel (2–4 nm) and optimum N content present in the sample. This work further demonstrated that the intelligent pre-design to modulate the porous channels and heteroatoms contents may result in the development of efficient electrodes towards energy storage devices.

In another aspect, the conductivity of CTFs can be enhanced by hybridizing them with appropriate carbonaceous materials. For example, Scherf *et al.*[99] prepared a composite of N-rich graphene and CTFs through a solution-based approach. The specific capacitances of as-produced GMP2NC reached a value of 273 F g^{-1} at 0.2 A g^{-1}, and 193 F g^{-1} at 5 A g^{-1} due to the high active area and short ion diffusion paths during the charge/discharge processes. Their reported capacitance of 70.7% retention when the current density increased from 0.2 to 5 A g^{-1} is higher than that of most of the corresponding materials in the literatures.

The large SSA and porosity of CTFs theoretically make them suitable for enhancing the SCs of electrodes. However, most of the reported CTFs exhibit low ionic and electrical conductivity, which limits their successful application. The addition of extra conductive components inevitably reduces the SSA of the composites. Alternatively, conductivity issues can be addressed by converting the CTFs into porous carbons, which can significantly increase their conductivity, while still maintaining the basic CTFs. The use of CTF-derived nanocarbons as electrode materials can improve the exposed surface areas, yielding relatively high capacitances. These observations make CTFs a

widely acceptable precursor to obtain carbonaceous materials with a large SSA. Additionally, choosing the desired CTFs can lead to the formation of carbonaceous materials with suitable structures depending on the regulation of the pyrolysis conditions.

Ren *et al.*[100] prepared an N-doped porous carbon material (NPCM) with significant porosity *via* the carbonization of pre-designed CTF precursors with a well-defined framework structure. The as-prepared material exhibited an acceptable specific capacitance of 264 F g^{-1} at the current density of 0.1 A g^{-1} and outstanding cycling stability. Similarly, Jian *et al.*[101] reported the preparation of a multi-heteroatom-doped porous carbon framework (MPCF) based on cyano groups under ionothermal conditions using 4,4′-(4-oxophthalazine-1,3(4*H*)-diyl)dibenzonitrile units. They reported that the resulting MPCF exhibited a high energy density of 65 W h kg^{-1} at 0.1 A g^{-1} and excellent stability of 98% capacitance retention after 10 000 cycles. Furthermore, Kuang *et al.*[102] prepared a novel fumaronitrile-derived FUM-CTF containing a super-rich N-content by carbonization, subsequently activating it at different temperatures using KOH. In this study, FUM-700, which corresponds to an activation temperature of 700 °C, demonstrated an ultra-high specific capacitance of 400 F g^{-1} at a current density of 1 A g^{-1} and a remarkable energy density of over 18 W h kg^{-1} in 6 M KOH electrolyte. In a further study, Shim *et al.*[103] converted a triazine-based polymer to a highly porous carbonaceous material *via* carbonization, and subsequently activated it through CO_2. The as-prepared nanocarbon exhibited a capacitance of 278 F g^{-1} at a current density of 1 A g^{-1} due to its large SSA (up to 2003 m^2 g^{-1}) and appropriate N loading (*ca.* 2 wt%). Similarly, Dutta *et al.*[104] carbonized triazine-based polyimide frameworks using $ZnCl_2$, exhibiting a large SSA of 1650 m^2 g^{-1}, ultra-high porosity and high N content of up to 6.3 wt%. Consequently, the optimal TPI-P-700 exhibited a specific capacitance of 423 F g^{-1} (at 1 A g^{-1}) and an excellent rate capability of 67% up to 20 A g^{-1} in a three-electrode system. Furthermore, Haldorai *et al.*[105] fabricated N-doped microporous carbon (N-MPC) *via* the carbonization of a novel CTF precursor, which led to a high SSA (801 m^2 g^{-1}) and uniform pore size in the sample. By using 6 M KOH electrolyte to study the performance of N-MPC, they obtained a high specific capacitance of 505 F g^{-1} at a current density of 0.5 A g^{-1}. Separately, Wei *et al.*[106] designed N-rich carbon by pyrolyzing blended triazine-conjugated microporous polymers with graphene aerogel. The resulting microporous carbon exhibited a significant increase in the supercapacitive performance, which was up to 325 F g^{-1} with an energy density of up to 12.95 W h kg^{-1} and good reusability of 99% capacitance retention after 10 000 cycles at 5 A g^{-1}.

Recently, Xia *et al.*[107] reported the carbonization of a triazine-based porous aromatic framework (LNU-18) to obtain N-rich carbonaceous materials. The resulting product demonstrated a maximum specific capacitance of 269 F g^{-1} at a current density of 0.5 A g^{-1}, which can be attributed to the suitable arrangements of N atoms (N triazine and N amine) in the porous carbons. Furthermore, Kuo *et al.*[75] prepared N-rich microporous carbon (N-DMC) using a template-free pyrolysis method and cross-linked CTF. The obtained N-DMC displayed an electrochemical capacitance of 185 F g^{-1} at a current density of 1.0 A g^{-1} and excellent stability after 4000 cycles (87% capacitance retention at 20 A g^{-1}). Ye *et al.*[108] prepared a porous CTF-based carbon (CTF-800) by ionothermal synthesis at 800 °C. This CTF-800 was used as an electrode material and a large specific capacitance of 628 F g^{-1} at 0.5 A g^{-1}, high rate stability (71% of capacitance retention at 50 A g^{-1}), and remarkable cyclic stability (96% capacitance retention over 20 000 cycles) in 1 M aqueous H_2SO_4 in a three-electrode system were observed. Meanwhile, the device with [EMIM][BF_4] electrolyte could operate well at various temperatures ranging from −20 °C to 60 °C with excellent performance for energy storage. In addition, Hu *et al.*[109] prepared pyridine-incorporated CTFs (p-CTFs) with a controlled N content through *in situ* ionothermal synthesis at different temperatures. The as-synthesized hierarchical porous carbon (p-CTF-800) exhibited the highest SSA value of 2795 m^2 g^{-1}, N content of 11.82 wt% and broad pore size distribution in the range of 0.65–5 nm. Owing to these attractive properties, p-CTF-800 attained a high specific capacitance of up to 406 F g^{-1} in acid electrolyte and a specific capacitance of 245.7 F g^{-1} in basic aqueous solution with an extraordinary energy density of 6.91 W h kg^{-1}. These works manifest that the introduction of pyridine rings in p-CTFs and subsequent pyrolysis to control the pore sizes at various temperatures can lead to high-performance SC electrode materials. In contrast to the literature, Duan *et al.*[110] reported a dual-step approach using ionothermal synthesis and partial pyrolysis in molten $ZnCl_2$ to synthesize porous carbonaceous materials. The as-obtained carbons exhibited excellent areal capacities of up to 2.27 F cm^{-2}. As displayed in Fig. 6, Jian *et al.*[111] constructed N,O-containing micro/mesoporous CTFs (p-TIDN@700) though ionothermal synthesis. The as-prepared p-TIDN exhibited a uniform O and N distribution together with micro-mesoporous nature, which exhibited a promising performance for energy storage and high cycling stability in 1 M H_2SO_4.

Furthermore, the SCs based on p-TIDN@700 displayed a high energy density (24.23 W h kg^{-1}) and high stability (only

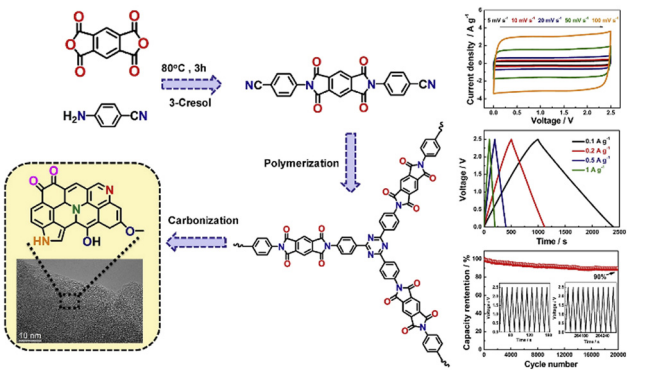

Fig. 6 Schematic of the synthesis of p-TIDN and the electrochemical performance of p-TIDN in a two-electrode system in $TEABF_4$/AN. Reproduced from ref. 111 with permission from Elsevier, Copyright 2020.

10% capacitance decay after 20 000 cycles at 10 A g^{-1}) in $TEABF_4$/AN system. Besides, the systematic analysis revealed that pyrrolic-N, pyridinic-N, and quinone-O are the most conducive species in energy storage. Wang *et al.* employed CTFs decorated with abundant F and N atoms as precursors to prepare porous carbonaceous materials with a large SSA *via* the *in situ* doping method.[112] The as-prepared carbon material possessed a large SSA ($\sim$1849.1 m^2 g^{-1}), specific capacitance value of 326 F g^{-1} at 1 A g^{-1}, and outstanding cyclability even after 10 000 cycles. This study provided insights into multi-heteroatom-doped carbons derived from CTFs *via* the *in situ* doping process.

As mentioned, CTF precursor materials have been successfully transformed into multi-functional porous carbons. The pore size can be theoretically pre-designed by choosing the desired monomers.[12] However, these carbonaceous materials are accompanied by the usual random morphology that comes from CTF precursors. Therefore, the direct pyrolysis of CTFs into well-ordered porous carbon nanosheets is challenging. Considering this, Yang *et al.*[113] synthesized graphene-linked CTFs (G-CTFs) containing an ultra-large SSA (1584 m^2 g^{-1}) by polymerizing *p*-benzenedinitrile and *p*-benzonitrile-linked reduced graphene oxide (rGO) in a molten state. The pyrolysis of the prepared material easily yielded N-rich porous carbon nanosheets (G-PCs). The G-PCs performed excellently in energy storage applications as an electrode in SCs (340 F g^{-1} at 0.1 A g^{-1} and 10 000 stable charge–discharge cycles at 5 A g^{-1}), demonstrating the viability of this method. The performances of CTF-based electrodes in SCs are summarized in Table 2.

3.1.2 Alkali-ion batteries. Research into the successful commercial applications of lithium-ion batteries (LIBs) can be traced back decades. However, the scarce availability of Li metal coupled with its high processing costs limit their large-scale applications. This challenge has become even more pronounced with the development of electric vehicles (EVs), which further increase the demands. Therefore, vast research attention has been focused on the exploration of suitable alternatives to Li recently.[114] Among the suitable candidates, sodium and potassium have garnered the most attention due to their low cost and widespread availability. They can be developed into sodium- and potassium-ion batteries (SIBs and PIBs, respectively), as alternatives to LIBs.[115] However, careful consideration must be given to developing new electrode materials that maintain their high potentials (Na: −2.71 V; K: −2.93 V; and Li: −3.04 V) and their large ionic radius.[116] The development of efficient electrodes based on these metals is of great importance for sustainable energy applications.

3.1.2.1 Lithium-ion batteries. LIBs mainly consist of three components, *i.e.*, cathode, anode and electrolyte.[117] At the anode, Li gets oxidized to Li^+ and travels through the electrolyte to the cathode. The most commonly used materials as the cathodes and anodes in practical LIBs are graphite and lithium cobalt oxide, respectively. However, the exploration of advanced materials to fulfil the demand of future energy-based applications is urgently required to counter the low theoretical capacities of graphite (372 mA h g^{-1}) and $LiCoO_2$ (148 mA h g^{-1}). In this regard, CTFs with ordered and functional pores serve as one of the most promising alternative materials, which is attributed to their suitability to store Li^+ ions and enhance the charge/discharge processes. Moreover, the heteroatom units in CTFs may also function as active sites for redox reactions during the electrochemical process. These aspects of CTFs have convinced researchers to explore their use as electrode materials for LIBs.

In 2012, Sakaushi *et al.* successfully employed amorphous CTF-1 as a cathode in LIBs and they observed a reversible capacity of about 160 mA h g^{-1}.[118] They also confirmed that the specific power could be tuned by choosing appropriate monomers and frameworks with desired functionalities.

Table 2 A comparison of the performance of CTF-based materials in supercapacitors

Sample	Electrolyte	Rate	Initial capacity (F g^{-1})	Cycles	Retention after cycles (%)	Ref.
Car-CTF	1 M KCl	0.2 mA cm^{-2}	—	8000	96	32
PTFs-700	$EMIMBF_4$	10 A g^{-1}	—	1000	85	86
TCNQ-CTF-800	1 M KOH	7 A g^{-1}	—	5000	92	87
CTF_{M-TFP}	2 M KOH	0.5 A g^{-1}	74.5	4500	96	88
Pyrene-CTFs	1 M KOH	10 A g^{-1}	—	2000	97	89
p-CTFs	1 M NaCl	1 mV s^{-1}	122.63	—	—	92
PDC-MA-CTF	6 M KOH	5 A g^{-1}	—	20 000	88	93
CTF-700	2.96 M $ZnCl_2$	1 A g^{-1}	154	—	—	95
TPT-DAHQ COF	1 M KOH	10 A g^{-1}	—	1850	98.8	91
TDFP-1	0.1 M H_2SO_4	10 A g^{-1}	—	1000	95	94
NPCM-1	6 M KOH	1 A g^{-1}	—	10 000	$\sim$100	100
MPCFs@700	1 M H_2SO_4	10 A g^{-1}	—	30 000	112	101
FUM-700	6 M KOH	10 A g^{-1}	400	10 000	95	102
AC-900	6 M KOH	2 A g^{-1}	278	3000	95	103
TPI-P-700	1 M H_2SO_4	30 A g^{-1}	—	10 000	$\sim$100	104
NMPC	6 M KOH	3 A g^{-1}	505	10 000	89	105
CMPs	6 M KOH	5 A g^{-1}	—	10 000	99	106
LNU-18-800	6 M KOH	2 A g^{-1}	—	5000	96.2	107
N-DMC	1 M KC	20 A g^{-1}	185	4000	87%	75
G-PCs	6 M KOH	5 A g^{-1}	340	10 000	—	113
CTF-800	1 M H_2SO_4	30 A g^{-1}	628	20 000	96%	108

These findings open a new avenue of using synthetic porous materials to enhance the performance of batteries. Similarly, Lotsch *et al.*[119] obtained a high reversible capacity (around 150 mA h g^{-1}) by using CTFs that were synthesized using various linkers. Xin *et al.*[120] developed an anthraquinone-triazine-based CTF, which served as an excellent anode, exhibiting high reversible capacities of 1770 mA h g^{-1} and 760 mA h g^{-1} at 200 mA g^{-1} and 1 A g^{-1}, respectively, together with superior recycling capacity.

Despite the promising activities of CTFs on the lab-scale, their severe agglomeration and stacking morphology are commonly observed, which greatly affect their performance and stability. Thus, to address this issue, the exfoliation of fluorinated CTF (FCTF) has been explored as an anode in LIBs. For instance, the exfoliated FCTF showed almost two-times the lithium storage capacity of its non-exfoliated counterpart (1035 mA h g^{-1} *vs.* 538 mA h g^{-1} at a current density of 100 mA g^{-1}).[121] Similarly, Fan *et al.*[122] observed an increase of ~380% specific capacitance after the exfoliation of f-CTF-1. It is worth noting that exfoliation enabled the exposure of a large number of active sites, which shortened the diffusion paths of Li^+ ions. Besides exfoliation, the incorporation of redox-active species in the CTF framework has also been explored to enhance the electrochemical performance of CTFs. Ruoff *et al.*[123] employed a redox-active anthraquinone-based CTF as an anode material and a remarkable rate with high specific capacities of 520 mA h g^{-1} up to 1500 cycles at 10C rate was reported. In another study, a cathode of methylene-decorated CTF exhibited a remarkable capacity of up to 247 mA h g^{-1} at 100 mA h g^{-1}.[124] This excellent activity can be attributed to the triazine radical intermediates, which facilitate the charging–discharging process, whereas methylene groups created additional redox active sites. Separately, Yang *et al.*[125] explored 3D cross-linked Azo-CTF as a cathode and a large reversible capacity of 205.6 mA h g^{-1} at a current density of 0.1 A g^{-1} was achieved, together with a long cycle life (89.1% capacity retention after 5000 cycles). The presence of electron-withdrawing/donating units in the framework can modulate the electronic structure for optimized conductivity and redox potentials. Distinctively, Dai *et al.* synthesized CTF-1 through a pre-polymerization step with CF_3SO_3H as the catalyst, followed by a polymerization step in molten $ZnCl_2$.[126] The attained CTF-1 displayed a super-lithiation performance, and both the triazine rings and benzene rings can store Li^+ ions in the form of Li_6C_6 or $Li_6C_3N_3$. Remarkably, the optimal CTF-1-400 showed a specific capacity of 740 mA h g^{-1} for 1000 cycles at 1 A g^{-1} with negligible capacity deterioration. To further understand the structure–property relationships concerning the super-lithiation performance of CTFs, Li *et al.* applied biphenyl-linked CTF-2 as the anode in LIBs, in which ultrahigh capacities (1526 mA h g^{-1} at 0.1 A g^{-1}) and excellent cycling stability were observed.[127] It is worth highlighting that the biphenyl units enriched CTF-2 with a plethora of lithium storage sites, ordered porous structures, and improved structural stability (Fig. 7).

To further disclose the potential application of CTFs, Sarkar *et al.* investigated the possibility of using a bilayer CTF as an anode material for LIBs using density functional theory (DFT) calculations.[128] The diffusion barrier, theoretical specific capacity, and average open-circuit voltage of the bilayer CTF were systematically investigated. It was found that the adsorption of Li atoms on the bilayer CTF is energetically favorable with a negative adsorption energy. The Li-decorated bilayer CTF exhibited metallic character, which is crucial for the high electrical conductivity of the anode material. Besides, in this study, the bilayer CTF exhibited a high theoretical specific capacity of 925.99 mA h g^{-1}, relatively low diffusion barrier of 0.65 eV, and high average open-circuit voltages (OCVs) of 1.58–0.51 V. The findings further support that the bilayer CTF can serve as a potential material for the anode of LIBs.

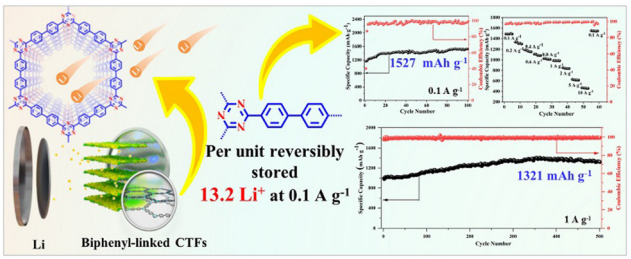

Fig. 7 Schematical illustration of the structure of a biphenyl-based CTF and its electrochemical performance. Reproduced from ref. 127 with permission from Elsevier, Copyright 2022.

To alleviate the insufficient conductivity of CTFs, Zhang *et al.* fabricated CTF-rGO composites after studying the growth compatibility of CTF with carbon nanomaterials.[129] By serving as the cathodes in LIBs, CTF-rGO delivered a large reversible capacity of 235 mA h g^{-1} in 80 cycles at 0.1 A g^{-1} and it maintained a capacity of 125 mA h g^{-1} after 1000 cycles at 2 A g^{-1}. The greatly improved performance in comparison to the unmodified pristine CTF evidenced the effectiveness of rational integration for the realization of SIBs with superior electrochemical performance. In addition to composites with a conductive matrix, the pyrolysis of CTFs is another effective strategy to improve their conductivity. Meanwhile, heteroatom doping of carbon materials can provide additional active sites for Li storage. CTF-derived porous carbon materials were reported by Feng *et al.*,[130] in which Si/N-doped porous carbon (Si@NPC) was prepared by carbonizing CTF-encapsulated Si nanoparticle composites for LIBs. As a favorable anode material for LIBs, Si@NPC delivered a high capacity (1390 mA h g^{-1} at 0.5 A g^{-1}), stable cycle performance (107% capacity retention for 200 cycles), and superior rate capability (420 mA h g^{-1} at 16 A g^{-1}). Here, the resulting carbon shell with sufficient porosity could relax the volume change of Si and endow more sites for Li^+ ion insertion, leading to high specific capacities and repeated usage. In a separate study, this research group prepared N-enriched porous carbon nanosheets (G-PCs) with a large SSA of 3021 m^2 g^{-1} by calcining graphene-coupled CTFs.[113] It was reported that graphene-coupled CTFs with typical 2D features provide more sites for Li^+ ion insertion/extraction and create more channels for the transportation of ion and charge. Consequently, the material possessed

a high reversible capacity of 235 mA h g^{-1} at 5 A g^{-1} for 3000 cycles.

3.1.2.2 Sodium-ion and potassium-ion batteries. Despite the wide use of LIBs in various electrochemical energy storage systems, the relatively scarce resource of Li metal restricts their large-scale applications.[131] As an alternative to LIBs, SIBs have recently attracted great research interest due to the vast natural reservoirs and standard electrode potential of Na.[13] However, the relatively large size of the Na^+ ion requires a host with a special network. Coincidentally, CTFs with intrinsic large pores make them ideal candidates for SIBs.

In 2013, Sakaushi *et al.*[132] reported the fabrication of a high-performance SIB device employing a dipolar CTF electrode, where a high specific power (10 kW kg^{-1}), specific energy (500 W h kg^{-1}), and cycle retention of over 7000 cycles were observed. Subsequently, CTFs became a topic of intensive research with the aim of developing high-performance organic electrodes for SIB devices. Xu *et al.* synthesized millimeter-size crystalline CTFs with a clear lamellar structure.[133] When they were explored as polymeric anodes for SIBs, the exfoliated 2D CTF exhibited a high capacity (262 mA h g^{-1} at 0.1 A g^{-1}), notable rate capability (119 mA h g^{-1} at 5.0 A g^{-1}), and exceptional cycling stability (95% capacity retention after 1200 cycles). Furthermore, Wang *et al.* synthesized exfoliated F containing CTF (E-FCTF) using a self-polymerization reaction and physically exfoliated method.[121] E-FCTF, which possessed strong triazine linkage and composed of few-layers, could promote the electrochemical kinetics and shorten the diffusion pathways of Na^+ ions, leading to improved active reactivity for Na^+ storage. Consequently, E-FCTF exhibited a good reversible capacity (332 mA h g^{-1} at 0.1 A g^{-1}) and cyclability (220 mA h g^{-1} after 200 cycles at 0.1 A g^{-1}). The results in this study signified the importance of appropriate exfoliation to improve the electrochemical performance. It is noteworthy that crystalline CTFs have also attracted much attention as organic anode materials for SIBs. As depicted in Fig. 8, Dai *et al.* first implemented a novel dual rate-modulation method for the development of crystalline CTFs.[134] Owing to the high crystallinity and redox-active rich triazine linkages, the resulting CTF anode exhibited a great performance for Na^+ storage, where a capacity of 239 mA h g^{-1} at 1.0 A g^{-1} was obtained after 200 cycles. This new protocol provides new opportunities for the synthesis of crystalline CTFs, and also broaden their energy-related applications.

In addition to the use of pristine CTFs for Na storage, CTF-derived carbonaceous materials with high SSA and electrical conductivity have also been demonstrated in SIBs as anode materials. Zhang *et al.* reported a template-based method to synthesize N, P, and F co-doped hollow carbon nanomaterials (NPF-HCN), which were derived from a CTF-based nanocomposite.[13] In this study, the porous nanostructures of NPF-HCN facilitated the injection of electrolytes, which reduced the diffusion barrier of Na^+ ions. NPF-HCN was employed as an anode in SIBs, which delivered an excellent initial capacity of 569.6 mA h g^{-1} at 1 A g^{-1} and outstanding cycling behavior with a high capacity of 220.3 mA h g^{-1} at 5 A g^{-1} after 5000 cycles. This work demonstrated that CTFs are also suitable to be used as precursors to yield multi-heteroatom-doped porous carbon materials for energy storage devices.

Furthermore, CTF-based materials were also reported as electroactive anodes for potassium-ion batteries (KIBs) for improved electrochemical performance. For instance, Wang *et al.*[121] introduced F atoms in CTFs to fabricate a 2D CTF, which was further exfoliated into few-layers and denoted as E-FCTF. The resulted E-FCTF anode exhibited an enhanced K^+ storage capacity of 228 mA h g^{-1} after 200 cycles at 0.1 A g^{-1}. The improved performance was ascribed to the synergistic effects of the electro-active triazine linkage, abundant porous structure, and presence of F atoms in the E-FCTF anodes. However, the effect of the CTF pore size on the electrochemical performance was not studied in this work. Zhu *et al.*[135] developed two homologous CTFs, which possessed similar chemical compositions but with various pore sizes to serve as the anode materials of KIBs. In this study, they revealed that the electrochemical performance is closely related to the pore size of the

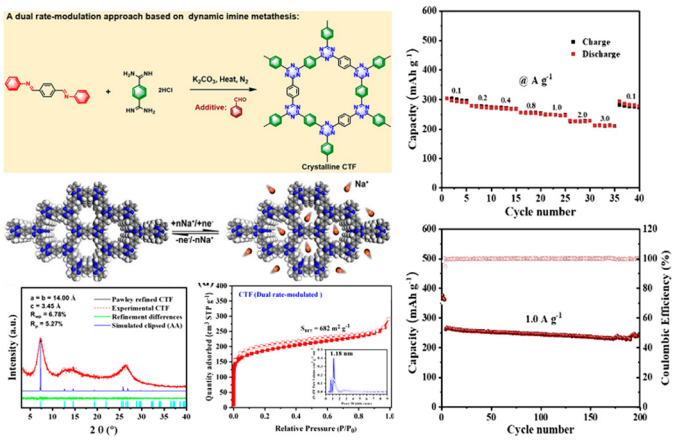

Fig. 8 Schematic diagram of a dual rate-modulation approach for the synthesis of crystalline CTF and its electrochemical performance. Reproduced from ref. 134 with permission from the American Chemical Society, Copyright 2022.

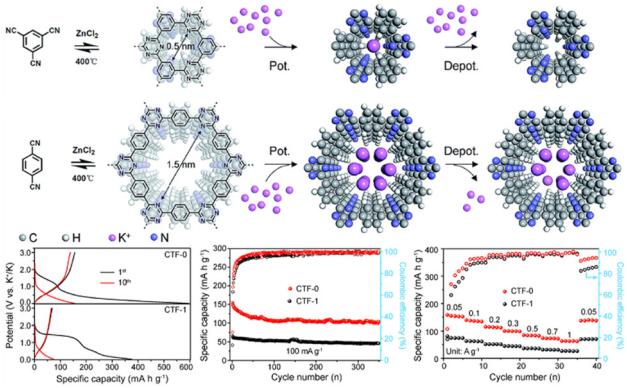

Fig. 9 Schematic illustration of the formation of CTFs and the corresponding potassiation/depotassiation process. The electrochemical performance of CTFs with different pore sizes is also included. Reproduced from ref. 135 with permission from The Royal Society of Chemistry, Copyright 2019.

framework. As demonstrated in Fig. 9, CTF-0 with a smaller pore size displayed a superior energy storage performance in comparison to CTF-1 with larger pore size. The ultramicropores in CTF-0 are favourable for the reversible transport of K^+, which enhanced the electrochemical performance. These findings provide insight into the rational design of anode materials for KIBs to achieve excellent energy storage performance.

3.1.3 Lithium–sulfur batteries. Lithium–sulfur batteries (LSBs) have been widely studied as efficient energy storage devices owing to their high theoretical capacity (1672 mA h g^{-1}) and energy density (2600 W h kg^{-1}).[136] More importantly, sulfur is inexpensive, abundant, and environmentally friendly.[137] These properties enable LSBs to serve as advanced energy storage devices. In LSBs, the intermediate products are termed polysulfides (Li_2S_x),[138] which are soluble in most solvents. However, after they move to Li anodes due to the shuttle effect, insoluble and insulating Li_2S will be formed, which lead to lower Coulombic efficiencies and poor recyclability. Therefore, the design of novel materials to host and retain the polysulfide intermediates together with high surface areas for electrochemical process is necessary.

The rational design of CTFs can provide a promising platform to store and immobilize sulfur and dissolve Li_2S_x. Typically, CTFs and sulfur powder are mixed and heated, and then sulfur is injected into the pores of CTFs. Therefore, CTFs with high porosities are crucial to encapsulate sulfur and the resulting polysulfides. In 2014, Wang *et al.* demonstrated a sulfur-based cathode for LSBs for the first time using CTF-1 as the host material.[139] The as-obtained cathode delivered a reversible capacity of 541 mA h g^{-1} at a very high rate of 1C. This finding clearly manifests that the incorporation of sulfur in the pores of CTFs can enhance the cyclic performance of LSBs. Inspired by this approach, Coskun *et al.*[16] developed sulfur-loaded CTF-1 (S-CTF-1). In this study, sulfur was not only physically loaded in the pores of CTF-1, but also covalently attached to CTF-1 during polymerization. The sulfur content in S-CTF-1 was as high as 62 wt%. Consequently, S-CTF-1 showed high cycling stability and a great rate performance, originating from the uniform sulfur distribution in the nanopores of the CTF-1 framework and the strong C–S covalent bonds. The major drawback of this work is that the C–S crosslinking inhibited a further increase in the sulfur content. In another work, Coskun and co-workers reported a fluorinated sulfur-rich CTF (SF-CTF) *via* the sulfur-mediated trimerization of tetrafluorophthalonitrile.[140] The sulfur content was close to 86 wt% due to the substitution reaction between the perfluoroaryl units and sulfur. When it was tested as a cathode material in LSBs, the SF-CTF electrode showed a great electrochemical performance, such as specific capacity of 1138.2 mA h g^{-1} at 0.05C, 93.1% initial Coulombic efficiency, and 81.6% capacity retention at 1C for 300 cycles. These results provided impetus for modulating the electrochemical performance of CTFs *via* rational design at the molecular level. In another study, Wang *et al.*[141] synthesized fluorinated sulfur-rich CTF (FCTF-S) *via* the one-step sulfur-mediated reaction of perfluorinated nitriles, which served as efficient sulfur immobilizers for LSBs. The presence of large pores and covalent sulfur bonding successfully trapped the sulfur to hinder the loss of Li_2S_x. As expected, FCTF-S exhibited a high capacity of 1296 mA h g^{-1} at 0.1C and a stable cycling performance of 833 mA h g^{-1} after 150 cycles at 0.5C. In a further study, Wang and Xu *et al.* prepared FCTFs and they were tested as hosts for sulfur migration at different incremental temperatures.[142] Due to the physical incorporation of sulfur inside the pores and the presence of chemically linked sulfur, the shuttle of Li_2S_x was effectively restricted. Besides, Kuang and co-workers[143] restricted sulfur moieties in highly fluorinated sulfur-rich multiple CTFs *via* a physical and chemical approach. The sample exhibited a specific capacity of 681 mA h g^{-1} and capacity retention of 62.6% after 400 cycles. The superior cycle performance was ascribed to the uniform sulfur distribution, C–S chemical bonding, and affinity of triazine rings for polysulfide. In addition, Kaskel *et al.*[144] further illuminated the applicability of CTFs as a potential cathode material in LSBs.

Despite the progress, few reports have focused on the structural design of heteroatom-containing linking units in CTFs to enhance the sulfur loading and electrochemical performance of LSBs. In this regard, Jian *et al.* reported the synthesis of two types of N,O-containing CTFs (NO-CTF-1 and NO-CTF-2) using N,O-containing linkers,[145] which were used as LSB electrodes to study the effect of N and O on polysulfide redox conversion reactions. The extra electron pairs on the N and O heteroatoms interacted with the Lewis acid of the terminal Li atoms in lithium Li_2S_x, resulting in NO-CTF-1 to deliver a high reversible capacity of 1250 mA h g^{-1} at 0.1C, excellent cycling stability with a capacity retention of 92% at 0.5C (300 cycles), and excellent rate performance of up to 678 mA h g^{-1} at 2C. Additionally, this study also researched the effect of heteroatom-containing building units on the charge and discharge process and provided powerful guidance for designing more CTF-based electrode materials. In another study, Zhao *et al.*[146] designed and synthesized a novel CTFO with plentiful N and O *via* the copolymerization of 2,4,6-triphenoxy-*s*-triazine and 2,4,6-trichloro-1,3,5-triazine using

Friedel–Crafts alkylation method. The presence of N and O strengthened the chemical fixing capability toward lithium polysulfide intermediates to prevent the shuttle effect. The S@CTFO electrode supplied an initial discharge capacity of 1074.5 mA h g^{-1} at the current density of 0.2C and a capacity of 853.2 mA h g^{-1} after 100 charge–discharge cycles with the Coulombic efficiency of 99.5%. These results confirm that the incorporation of multiple heteroatoms can reduce the shuttle effect and improve the performance of LSBs.

In comparison to single CTFs, CTF-based composites exhibit enhanced electrochemical performances after the addition of other functional components. For example, Yang and co-workers[136] synthesized layered CTF on Ti_3C_2 MXene nanosheets (CTF/TNS) with 2D heterostructures as a sulfur host for LSBs (Fig. 10). The concomitant effects of highly ordered CTF and highly conductive TNSs rendered the resulting hybrid suitable for a high sulfur loading to efficiently transport electrons and ions. Additionally, the lithium-philic N sites in CTF and sulfur-philic Ti sites in TNSs enabled dual-site chemical linking of Li_2S_x to effectively reduce the shuttle effect. The S@CTF/TNS cathode with a high sulfur content (76 wt%) exhibited a large reversible capacity (1441 mA h g^{-1} at 0.2C), exceptional cycling stability (up to 1000 cycles at 1C with a 0.014% capacity decay rate per cycle), and outstanding rate capability. This study provided insight into the development of ideal CTF-based nanocomposites with desirable properties and structures for LSB applications. Meng and co-workers[147] further reported a new type of hybrid conductive CTF-rGO mediated by the sulfur cyclization of dinitrile monomers to realize S/P-CTF@rGO composites. The pores in CTF ensure the effective trapping of sulfur species, whereas rGO enhanced the transportation of electrons owing to its conductive nature, thereby accelerating the electrochemical process. The S/P-CTF@rGO cathode exhibited a high initial specific capacity of 1130 mA h g^{-1} at 0.5C and great capacity retention of 81.4% after 500 cycles, indicating only 0.04% degradation per cycle.

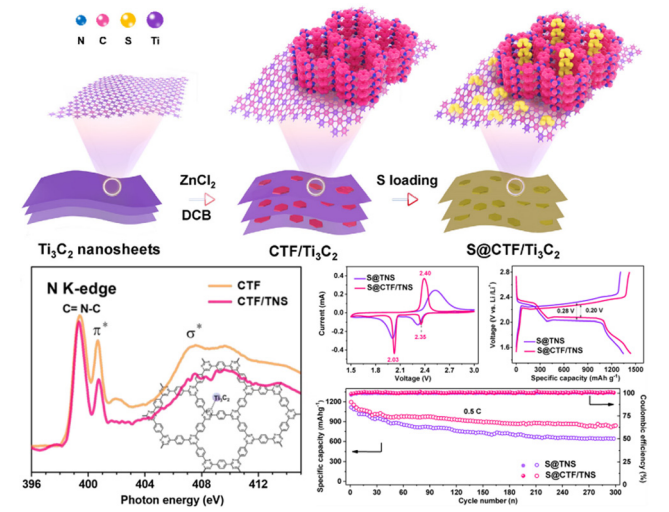

Fig. 10 Schematic illustration of the synthesis of 2D CTF/TNS heterostructures and the Li–S electrochemical performance of the composites. Reproduced from ref. 136 with permission from Elsevier, Copyright 2020.

Li_2S_x shuttling can be mitigated by trapping Li_2S_x through various interactions. For example, Choi *et al.* incorporated 1D charged polypyrrole into a 2D CTF (cPpy-S-CTF) in the presence of elemental sulfur for attaining a sulfur loading of about 83 wt%.[148] The resulting composite exhibited an outstanding electrochemical performance with a specific capacity of 1203.4 mA h g^{-1} at 0.05C, initial Coulombic efficiency of 94.1%, and capacity retention of 86.8% after 500 cycles. Notably, this strategy represents a significant breakthrough in addressing the challenges associated with CTFs, such as low electronic/ionic conductivity at considerable sulfur loadings.

2D CTFs can also be used as a functional coated-barrier to actively reduce the shuttling effect. Ye *et al.*[149] demonstrated that CTF-coated Celgard possesses high Li-ion diffusion properties for LSBs (Fig. 11). Notably, the easily prepared interlayers showed improved material utilization, cycle stability, rate capacity, anti-self-discharge behaviour and protection of the Li-anode. The same group also developed an ultralight functional separator through the electrostatic layer-by-layer assembly of functional-CTF and conductive polymer to effectively suppress the shuttle effect and improve the utility of sulfur towards enhanced LSB performances.[150] The barrier assembled with S-cathode and Li metal anode displayed promising cycling stability (0.052% capacity fade-rate per cycle over 1000 cycles at 1C), excellent utilization of sulfur (90.7% at 0.1C and 59.2% at 2C), and improved protective capability of the Li metal. The outstanding battery performance and facile large-scale

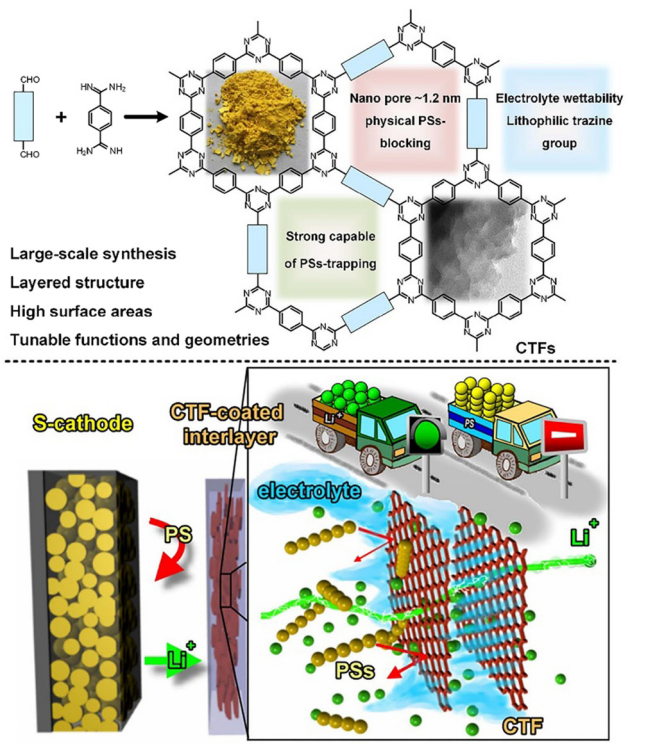

Fig. 11 Schematic diagram of CTF-coated interlayer design to simultaneously inhibit polysulfide shuttle and improve Li-ion transport in LSBs. Reproduced from ref. 149 with permission from Wiley-VCH, Copyright 2019.

Table 3 Electrochemical performance of CTF-based electrode materials for use in different types of batteries

Samples	Types of batteries	Condition	Specific capacity (mA h g^{-1})	Cycles	Ref.
G-PPF-p-400-600	LIBs	5 A g^{-1}	395	5100	209
Si@NPC	LIBs	1 A g^{-1}	1372	200	130
G-PCs	LIBs	5 A g^{-1}	235	3000	113
E-CIN-1	LIBs	0.1 A g^{-1}	1005	250	210
BPPF	LIBs	1 A g^{-1}	—	1000	211
CTF-rGO	LIBs	5 A g^{-1}	127	2500	129
Bilayer CTF	LIBs	—	—	—	128
P-MCN-1	LIBs	20 A g^{-1}	274	2500	212
CMPs	LIBs	5 A g^{-1}	326	1500	213
DAAQ-ECOF	LIBs	0.5 A g^{-1}	104	1800	214
CTF1	LIBs	—	—	—	119
E-FCTF	LIBs	2 A g^{-1}	581	1000	121
ACTF-1	LIBs	5 A g^{-1}	—	1000	118
PAT electrode	LIBs	1 A g^{-1}	760	400	120
TPI-P-700	LIBs	1 A g^{-1}	650	500	122
CTF-rGO-400-600	LIBs	5 A g^{-1}	127	2500	129
BPOE	SIBs	—	—	—	132
Exfoliated 2DP	SIBs	1 A g^{-1}	188	1200	133
CTF-0	KIBs	0.1 A g^{-1}	113	200	135
CTP-1	LSBs	1C	—	800	215
cPpy-S-CTF	LSBs	0.5C	610.1	500	148
S/P-CTF@rGO	LSBs	0.5C	920	500	147
S@CTF-Mono	LSBs	0.1C	1046	200	144
COF-F-SeS_2	LSBs	1C	520	200	216
FCTF-S	LSBs	0.5C	833	150	141
SF-CTF-1	LSBs	5C	330.3	300	140
CTF-celgard	LSBs	1C	—	800	149
TBP-80S	LSBs	5C	440	650	217
HCPT@COF	LSBs	0.5C	875	800	218
S-CTF-1	LSBs	1C	482.2	300	16
S/FCTF-400	LSBs	0.5C	494	200	142
FMCTF-S	LSBs	1C	426	400	143

production ability of this method offer an effective approach to address the various challenges presented by LSBs. Table 3 summarizes the experimental data of various batteries composed of CTF-based materials.

3.2 Electrochemical energy conversion

3.2.1 Oxygen reduction. Developing highly efficient and stable catalyst materials for the cathode oxygen reduction reaction (ORR) is a crucial challenge for advancing the application of fuel cells and metal–air batteries. Presently, most commercial systems heavily rely on platinum (Pt)-based catalysts. However, Pt is an expensive noble metal, and it leads to the formation of toxic intermediate products, which hinder its large-scale application. Therefore, the development of noble metal-free or even metal-free catalysts is of paramount significance. It is noteworthy that CTF materials can be synthesized through a convenient and controllable synthesis platform, in which chemical controllable means can be used to tailor specific structural CTFs with designed active centres. Besides, high-temperature pyrolysis of the CTF precursors can lead to the formation of abundant novel electrocatalytic-active carbon materials. As a metal-free electrocatalyst, the performance of the active site in porous polymers containing triazine is mainly determined by the pyridinic-N. Numerous studies have shown that the percentage of N atoms in the C-grid and the type of N (pyridinic-N, pyrrolic-N, and graphitic-N) crucially influence the electrocatalytic performance, and pyridinic-N is one of the best active sites for ORR catalytic performance.[151] Therefore, CTFs are widely used to catalyze the ORR reaction.[152] Table 4 summarizes the ORR performance of some reported CTF-based electrocatalysts.

Table 4 ORR performances of CTF-based electrocatalysts

Catalyst	Electrolyte	E_{onset} (V *vs.* RHE)	$E_{1/2}$ (V *vs.* RHE)	Ref.
Trz-COP	0.1 M KOH	—	0.73	4
Cu-CTF/CP	Saturated PBS	0.81	—	158
TTF-F	0.1 M KOH	0.822	0.767	219
CTF-CSU1	0.1 M KOH	0.79	0.57	154
CoSAs/PTFs	0.1 M KOH	—	0.808	187
Co_3O_4/CTF700	0.1 M KOH	—	0.84	162
Cu-S-CTF/CP	0.1 M PBS	0.62	—	159
CTF-Super P	0.1 M KOH	0.981	0.883	164
	0.1 M $HClO_4$	0.840	0.717	
TetCB–Fe/N/S/C	0.1 M KOH	1.018	0.908	18
	0.1 M $HClO_4$	0.899	—	
Fe@NCNT	0.1 M KOH	1.021	0.851	208
cCTN	0.1 M KOH	0.75	—	156
NHC/rGO-950	0.1 M KOH	0.95	0.83	17
FB7	0.1 M $HClO_4$	—	—	19
FeNC-900	0.1 M KOH	1.00	0.878	171
	0.1 M $HClO_4$	0.85	0.72	
PTF-Fe-I	0.1 M KOH	0.95	0.85	174
	0.1 M $HClO_4$	0.85	0.70	
Co/N-PC-900	0.1 M KOH	0.91	0.83	175
BINOL-CTF	0.1 M KOH	0.793	0.737	205
Co-CTF/KB	0.1 M KOH	0.940	0.830	161
NPS-800	0.1 M KOH	—	—	170
h-FeNC	0.1 M KOH	0.996	0.883	172
CTF DCBP-750	0.1 M KOH	0.9	0.79	155
HAT-CN-Co/C-800	0.1 M KOH	0.972	0.895	176
Trz-COP	0.1 M KOH	—	0.73	4
Pd@CTF	0.1 M KOH	—	0.872	206
ACTF-α-T	0.1 M KOH	~0.96	0.86	166
N/S-$HMCS_{900}$	0.1 M KOH	0.99	0.85	165
N-HCNF-2-1000	0.1 M KOH	1.01	0.84	207
NPF@CNF-800	0.1 M KOH	0.97	0.85	169
PC-900a	0.1 M KOH	0.866	0.871	167
NPF-CNS-2	0.1 M KOH	0.93	0.81	168
	0.1 M PBS	0.70	0.58	
	0.5 M H_2SO_4	0.83	0.70	

In 2014, Hu *et al.* synthesized CTFs and they were employed as ORR metal-free catalysts, which exhibited outstanding electrocatalytic activity in alkaline media.[153] In this study, artificial defects were introduced in the carbon framework *via* N-doping, which increased the electron delocalization due to the good electron-donating properties of the N atom, thereby promoting its ORR electrocatalytic activity. These findings demonstrated that CTFs with a high content of pyridinic-N have great potential in the field of energy-related electrocatalytic reactions. Besides, Yu *et al.* designed carbazole-based CTFs (CTF-CSUs) to catalyze the ORR under alkaline conditions.[154] The resultant catalyst exhibited attractive ORR activity, which is comparable to that of commercial Pt/C catalysts. Its excellent performance was attributed to its high content of N (15.33 wt%), large SSA (982 m^2 g^{-1}), and robust synergistic effects, resulting from the triazine and carbazole moieties. Furthermore, Palkovits *et al.* studied the effects of monomer and temperature on the framework functionalization and its ORR performance.[155]

The authors observed that a high synthesis temperature led to high ORR activity due to the transformation of pyridinic-N to graphitic-N, which rendered enhanced conductivity, SSA, and pore volume. This study also emphasized that graphitic-N is the active site rather than pyridinic-N for the binding and activation of O_2. Based on the previous progress, Wen and Yang *et al.* designed a 2D redox-active cationic CTF to serve as an ORR electrocatalyst for the formation of H_2O_2.[156] The experimental findings demonstrated that this electrocatalyst exhibited excellent ORR activity and high selectivity towards H_2O_2 (~85%). As mentioned previously, a high content of pyridinic-N in CTF will be beneficial for enhancing the ORR activity. Notably, this work also provided an innovative strategy to construct highly selective CTF-based electrocatalysts for the production of H_2O_2 from O_2.

Owing to the intrinsic poor conductivity of CTFs, their ORR performance is unsatisfactory when they are directly used as electrocatalysts. Exploring efficient ORR electrocatalysts to replace the expensive Pt-based catalysts requires the appropriate blending of conductivity and catalytic activity. In this regard, Nakanishi *et al.* successfully synthesized Pt-modified CTF/conductive carbon nanocomposites (Pt-CTF/CP) by inserting carbon nanoparticles at the polymerization stage of CTFs.[157] The as-prepared Pt-CTF/CP exhibited good ORR electrocatalytic activity in an acidic solution with high methanol tolerance. This result indicate the potential applications of CTFs as a cathode material in direct methanol fuel cells. Instead of precious metals, Cu and other transition metals can also be introduced in CTFs to improve their ORR performance. Kamiya and Hashimoto *et al.* demonstrated that composites of Cu-modified CTF and carbon nanoparticles can serve as efficient ORR electrocatalysts in neutral solutions.[158] Their findings suggest that a significant increase in ORR activity for CTFs can be achieved through the rational screening of the underlying framework. In another study, they also synthesized a Cu-incorporated S-linked CTF to function as an electrocatalyst for the ORR in neutral solution.[159] Besides, the dispersion of atomic transition metals in CTFs has also been developed to enhance their electrocatalytic activity for the ORR. For example, Cao and co-workers reported an ionothermal method to fabricate an Fe–N_x-containing CTF with a high Fe loading (up to 8.3 wt%).[160] Due to the large exposure of single-atom Fe–N_4 active sites, highly ordered pores, and great conductivity, the resulting catalyst exhibited superior ORR activity and excellent stability under both alkaline and acidic conditions. In another study, Zhi and Ma *et al.* prepared single cobalt atoms immobilized by CTFs with Ketjen Black hybridization (Co-CTF/KB) for the ORR.[161] Consequently, the as-prepared Co-CTF/KB exhibited remarkable ORR activity with an onset potential (E_{onset}) of 0.940 V, half-wave potential ($E_{1/2}$) of 0.830 V, high limiting current density (J_L) of 6.14 mA cm^{-2}, and low Tafel slope of 65 mV dec^{-1}, outperforming the commercial Pt/C. Besides, Fan *et al.* prepared a hybrid Co_3O_4/CTF ORR catalyst *via* a hydrothermal approach.[162] The obtained catalyst showed remarkable electrocatalytic ORR activity ($E_{1/2}$ of 0.84 V, J_d of 5.43 mA cm^{-2} and Tafel slope of 44.0 mV dec^{-1}), high stability, and excellent methanol resistance compared to the commercial Pt/C.

In addition to composite metals, the direct carbonization of CTF-based nanomaterials to create porous nanostructured carbons is another effective strategy to improve the conductivity, thereby improving their ORR electrocatalytic performance. Electrochemical studies showed that nanocarbons derived from CTFs possess several unique properties, as follows: (1) CTFs are composed of highly conjugated carbon skeletons and contain abundant heteroatoms, which can be used as ideal precursors for the preparation of functional heteroatom-doped carbon materials; (2) functional carbon-based materials with unique micromorphology can be obtained by regulating the micro–nano structure of CTF precursors; (3) CTFs possess highly ordered chemical structure and uniform heteroatom distribution in the framework, thus uniformly distributed heteroatom active centers can be obtained in the resultant nanocarbons by simple calcination. Benefiting from the rich hetero-element composition, hierarchically porous structure and unique micro/nano morphology of CTFs, the nanocarbons derived from CTFs exhibit outstanding performance in emerging electrocatalytic ORR fields.

Even without the assistance of metals, nanocarbons derived from CTFs can also be independently used as efficient ORR electrocatalysts. The N-rich CTF network has been explored for carbonization at 900 °C to prepare metal-free N-doped carbon materials for the ORR in alkaline media.[163] In 0.1 M KOH aqueous solution, the obtained NC-900 exhibited an E_{onset} and J_L of 0.972 V *vs.* RHE and 5.0 mA cm^{-2}, respectively, which are comparable to that of the commercial 20% Pt/C catalyst. In another work, Fan *et al.* prepared N-doped hierarchical porous carbons by optimizing the ratio of Super P in the nitrile linkers.[164] The resultant CTF-Super P-10 demonstrated a superior ORR performance in both alkaline and acidic electrolytes. The excellent performance mainly originated from the hierarchical pores, which acted as interconnected channels to afford the fast delivery of reactants and facilitate the discharge of the product. Liu *et al.* fabricated N and S co-doped hollow mesoporous carbon spheres from a sulfur-bridged CTF sphere *via* a novel template-free pyrolysis approach, in which superior ORR electrocatalytic activity was observed.[165] In addition, as displayed in Fig. 12, Jiang *et al.* synthesized a sheet-shaped NHC/rGO-950 composite with predominant pyridinic-N and graphitic-N integration through the carbonization of an

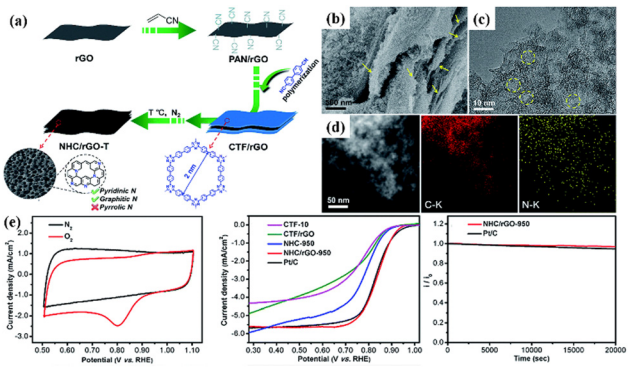

Fig. 12 (a) Schematic illustration of the fabrication of CTF-derived sandwich-like NHC/rGO-T layered composite. (b–d) Morphology features and (e) ORR performance of NHC/rGO-950. Reproduced from ref. 17 with permission from The Royal Society of Chemistry, Copyright 2017.

rGO-templated CTF precursor.[17] Owing to the synergistic effect between CTF-derived carbon and rGO, the layered NHC/rGO-950 exhibited an admirable ORR performance, ultrahigh stability and exceptional methanol tolerance. The inexpensive raw materials, facile fabrication and outstanding ORR electrocatalytic performance of the CTF-derived nanocarbon make it a very promising cathode material in fuel cells and metal–air batteries.

In another study, Zhuang *et al.* designed two N-doped different porous carbons by pyrolyzing two types of new isometric CTFs with adjustable structures using isometric cyano-based monomers.[166] As ORR electrocatalysts, the optimal ACTF-α-900 showed an admirable ORR performance with $E_{1/2}$ of 0.86 V and Tafel slope of 65 mV dec^{-1} in alkaline media, which is superior to other N-doped carbon nanocatalysts. Besides, the transformation of a novel CTF-Azs from porous polymer to porous carbons was also reported.[167] Owing to the azulene-type topologic defects, abundant N doping, large SSA, and lower charge-transfer impedance, the prepared porous carbons demonstrated good electrocatalytic activity in the ORR process.

Designing multi-heteroatom-doped carbon with excellent ORR electrocatalytic performances is highly desirable. In this regard, Liu *et al.* prepared N, P, and F co-doped carbon nanospheres using a heteroatom-enriched CTF as a ''self-doping'' precursor containing C, N, P, and F elements simultaneously. This approach avoided the dull and inefficient post-synthetic doping procedures.[168] In this work, introducing F enhanced the surface wettability and electronic structures of the as-prepared catalyst, which improved the overall ORR electrocatalytic performance. Notably, the improved carbon catalyst exhibited superb electrocatalytic ORR activity and prolonged durability in pH-universal conditions. Besides, they further prepared nanoflower-structured CTFs through polycondensation reaction triggered by ultrasound, and subsequently carbonized them to graphitic carbons with rich N, P, and F heteroatom-doped active centers.[169] Consequently, the developed electrocatalyst exhibited remarkable ORR activity ($E_{1/2}$ = 0.85 V *vs.* RHE) and remarkable cycling stability, outperforming most of the metal-free carbon electrocatalysts reported in the literature to date. Similarly, N, P, and S co-doped porous carbons were prepared from N, P, S-enriched CTFs.[170] The resultant carbon delivered outstanding quasi-four-electron ORR activity, high stability, and good methanol resistance in an alkaline medium, displaying its feasibility for use in diverse energy conversion devices.

The incorporation of metal components in CTFs allows the synthesis of porous carbons containing residual metal participators to further enhance their ORR electrocatalytic performance. For example, Cheng *et al.* synthesized an Fe/N-doped carbon catalyst with 3D hierarchically micro/meso/macro pores and large SSA *via* the carbonization of CTF-1 and $FeCl_3$ composites.[171] The resultant FeNC-900 electrocatalyst exhibited outstanding ORR behaviour with an $E_{1/2}$ of 0.878 V and 0.72 V in a wide pH range. The highly active CTF was used as a precursor for preparing Fe–N_x–C catalysts for the ORR in fuel cells.[19] The ORR activity was reflected by the porous and high density of active sites. Li *et al.* developed Fe–N-doped ordered mesoporous carbon nanocatalysts from CTF-based composites for the ORR in acidic and basic media.[172] The developed material in this study exhibited superior catalytic ORR activity in 0.1 M $HClO_4$ solution in comparison to that of commercial Pt/C. Li *et al.* prepared Fe–N_x/C materials from Fe-doped CTFs, which exhibited extraordinary ORR activity in both alkaline and acidic solution.[172,173] The authors proposed that Fe catalyzed Fe-doped CTFs to create extra Fe–N_x active sites. In addition, Zhang *et al.* prepared a series of CTFs co-decorated with Fe and I, and the derived carbon catalysts exhibited a high ORR performance in both basic and acidic conditions.[174]

Replacing Co with Fe in CTFs has also been studied. Lu *et al.* fabricated Co–CTF with a well-defined Co–N_4 center *via* ionothermal polymerization.[175] Co-CTF was directly pyrolyzed to form Co/N-anchored porous carbons, which exhibited a large SSA (874–987 m^2 g^{-1}) and uniform dispersion of the Co species. These Co/N-PCs showed good ORR activity with a positive E_{onset} of 0.91 V and $E_{1/2}$ of 0.83 V in 0.1 M KOH. In another study, a high-performance Co, N-doped carbon ORR catalyst was developed using an inexpensive and N-rich CTF precursor in alkaline media.[176] This work further demonstrates that CTF-based nanomaterials can be used as attractive precursors to prepare highly efficient metal-based N-doped carbon catalysts.

3.2.2 Oxygen evolution. Efficient OER electrocatalysis is important for a myriad of energy-related applications, including rechargeable metal–air batteries and electrocatalytic water splitting.[177] Previously, various metal oxides, such as IrO_x and RuO_x, have been explored as commercial OER electrocatalysts. Nevertheless, the high cost and scarcity of these metals make the corresponding catalysts unsuitable for large-scale production.[178] Hence, alternative non-metal-based catalysts such as CTFs have attracted great interest from the research community as next-generation electrocatalysts.

Kathiresan *et al.* synthesized a CTF by reacting cyanuric chloride with 1,4-phenylenediamine, and the obtained CTF presented decent electrocatalytic activity for the OER.[179] Furthermore, Janiak and co-workers applied an Ni nanoparticle supported-CTF in OER electrocatalysis.[180] In this work, Ni-CTFs exhibited a good electrochemical performance for the OER (reaching 10 mA cm^{-2} with an overpotential of 374 mV) due to their outstanding O_2 accessibility and good conductivity. As depicted in Fig. 13, Wang *et al.* prepared an Ru nanoparticle-loaded defective CTF (Ru/D-CTF).[181] After the calcination of the resultant Ru/D-CTF in air, it exhibited an excellent OER overpotential of 190 mV at 10 mA cm^{-2}.

Defect engineering and heteroatom doping have been reported as effective strategies to achieve more OER active sites in metal-free carbon-based materials.[182] In this regard, CTFs are frequently used as precursors.[169] Porous metal-free N-doped carbon can be prepared by directly carbonizing CTFs, as reported by Kathiresan *et al.*[183] The as-obtained material exhibited an excellent OER overpotential of 297 mV at a benchmark current density of 10 mA cm^{-2}.

3.2.3 Hydrogen evolution. Hydrogen, an abundant, clean, and renewable form of energy, is considered an ideal energy

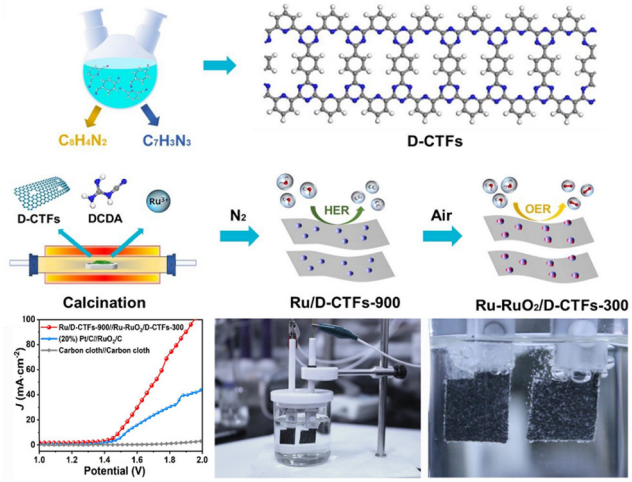

Fig. 13 Schematic illustration of the synthesis of D-CTF-based material and its OER electrochemical performance. Reproduced from ref. 181 with permission from Elsevier, Copyright 2020.

source for the fulfilment of future energy demand.[184] To date, Pt-based catalysts are commonly employed for the hydrogen evolution reaction (HER) owing to their fast kinetics and low overpotentials.[185] However, the high cost and scarce resource of Pt make Pt-based catalysts unsuitable for mass application. Therefore, alternative materials are highly sought after. Sarkar *et al.* predicted that some heteroatom-doped bipyridine-linked CTFs can serve as remarkable electrocatalysts for the HER based on DFT simulations.[186] Thus, the development of HER electrocatalysts from CTFs is worth exploring.

Cao *et al.* reported the synthesis of various cobalt single-atom affixed porous porphyrinic CTFs (CoSAs/PTF) *via* the ionothermal method, as shown in Fig. 14.[187] Due to the presence of large Co–N_4 moieties, ordered porous network, and excellent conductivity, the resulting material exhibited optimal HER activity with a small onset potential of 21 mV and low Tafel slope of 50 mV dec^{-1}. Hu *et al.*[188] synthesized an HER electrocatalyst through the electrostatic assembly of a polyoxometalate

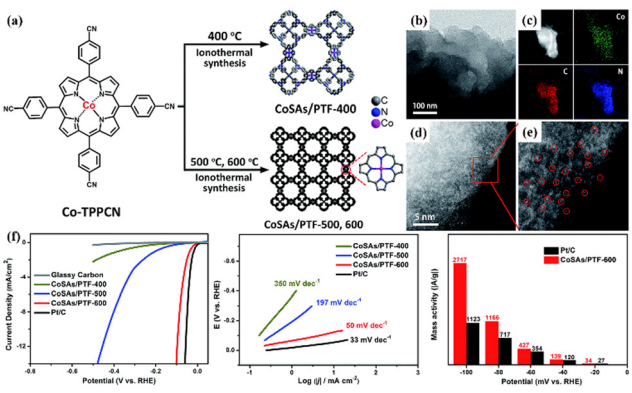

Fig. 14 (a) Schematic illustration of the fabrication of CoSAs/PTFs. (b–e) STEM images of CoSAs/PTF-600. (f) HER electrochemical performance of CoSAs/PTFs and Pt/C. Reproduced from ref. 187 with permission from The Royal Society of Chemistry, Copyright 2019.

with a porous cationic CTF. The resulting $PMo_{10}V_2$@CTF demonstrated high activity for electrocatalytic H_2 production. Han's group studied two CTFs with different pore structures (single-pores and hetero-pores) for electrocatalytic activity.[189] Subsequently, the performance of the two CTFs were improved through metal ions/clusters and these modified CTFs were evaluated as HER electrocatalysts in an acidic medium. Consequently, DCP-CTF-Pt^{2+} displayed the optimal electrocatalytic activity with an overpotential of 46 mV and small Tafel slope of 30.2 mV dec^{-1}, which are comparable to the state-of-the-art activity exhibited by Pt/C.

In addition, composites of CTF and metals species were also studied as electrocatalysts for the HER. For example, Hu's group synthesized MoS_2 nanoparticles decorated with high-quality crystal CTF for efficient HER electrocatalysis.[190] In this work, the intrinsic p-conjugated ordered channels in CTFs provide multi-functional backing for electron transport and mass diffusion in the HER process. It is worth noting that the CTF@MoS_2 sample exhibited superior catalytic kinetics with an overpotential of 93 mV and a small Tafel slope of 43 mV dec^{-1}, which is superior to most reported analogous catalysts. These findings elucidate that proper attention to CTF-based materials is required for the development of highly efficient electrocatalysts for advanced HER.

3.2.4 Carbon dioxide reduction. The rapid increase in the global CO_2 concentration has led to various disastrous environmental issues, such as climate change, polar ice melting, and species extinction.[191] The conversion of CO_2 into value-added carbon-based fuels is regarded as a promising and sustainable approach to reduce the CO_2 concentration.[192] In this context, CTF-based materials have also been studied as CO_2 reduction reaction (CO_2RR) electrocatalysts for the formation of value-added products from the unwanted CO_2.

To the best of our knowledge, CTF catalysts with rich pyridinic-N doped active sites were first reported for the CO_2RR in 2018.[193] The prepared catalyst could selectively reduce CO_2 into CO with a desirable faradaic efficiency (FE) of ~82% under a mild overpotential of 560 mV. This study opens up a pathway for the rational design of porous CTFs for electrocatalytic CO_2RR. Subsequently, a perfluorinated CTF was reported as a highly active electrocatalyst with high selectivity for CO_2 conversion into CH_4 with an FE of 99.3% in water.[194] In another study, a boron-doped CTF was also studied for the electroreduction of CO_2 into CO.[195] The authors found that doping with boron significantly boosted the CO selectivity to 91.2%. CTF/carbon nanotube hybrids were also demonstrated to be an efficient electrocatalyst for the CO_2RR, producing CO with an FE of up to ~81%.[196] They found that modifying the surface of the carbon nanotubes with hydroxyl groups could promote an intimate connection between the CTF and carbon nanotubes, thus facilitating electron transfer during the CO_2RR process.

The modification of CTF with metals (Cu, Ni, Co, *etc.*) also serves as an effective approach to regulate the electrocatalytic CO_2RR.[197–200] For example, Zhuang *et al.* fabricated an Ni porphyrin-based CTF (NiPor-CTF) with atomically dispersed NiN_4 centers, which displayed great catalytic behaviors for

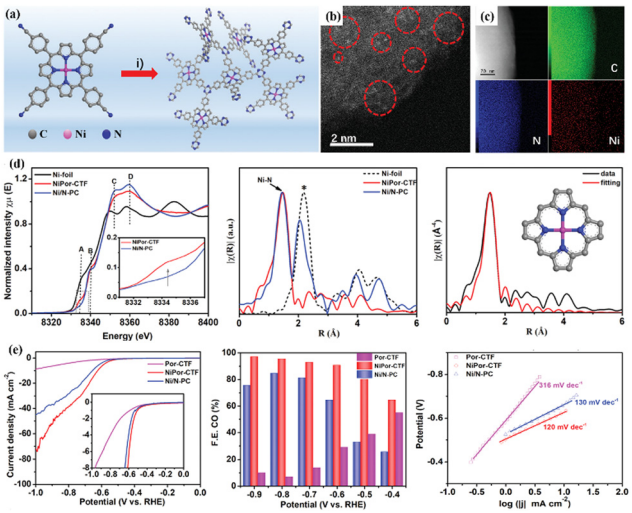

Fig. 15 (a) Schematic diagram for the synthesis of NiPor-CTF through ionothermal strategy. (b and c) HAADF-STEM and elemental mapping, (d) corresponding EXAFS spectra, and (e) CO_2RR performance of NiPor-CTF. Reproduced from ref. 201 with permission from Wiley-VCH, Copyright 2019.

electrocatalytic CO_2RR to CO with an FE of 97% at an applied potential of −0.9 V with a high current density of 52.9 mA cm^{-2}.[201] This excellent performance can be attributed to its atomically distributed NiN_4 centers (Fig. 15). In an independent study, a highly crystalline CTF with isolated Ni single-atom electrode was also demonstrated to display high activity, selectivity, and stability for CO production from CO_2, achieving a high FE of 97.5% at −0.52 V.[202]

Besides decorating with Ni, Cu-confined CTFs were also reported as active electrocatalysts for the CO_2RR with high reduction efficiency at relatively low overpotentials. Yang *et al.* developed a Cu-based CTF (CTF-Cu) featuring a CuN_2Cl_2 structure.[203] By designing CTF with bipyridine units, CO_2 could be reduced into hydrocarbon products over CTF-Cu with a maximum FE of 81.3% at a negative potential. Further probing research of the CO electro-reduction verified that CO is one of the primary intermediates for the CO_2RR. Furthermore, imidazolium-functionalized CTF-stabilized Cu nanoparticles (Cu/ICTF) were also reported for enhanced electrocatalytic CO_2RR to produce ethylene.[204] The developed Cu/ICTF produced a higher FE than the unmodified Cu/CTF due to the improved CO_2 capture capacity and reduced energy barrier for the activation of CO_2.

The electrochemical CO_2RR is a promising avenue to store energy from intermittent power sources and synthesize carbon-containing feedstocks (*e.g.*, CO, CH_4, C_2H_4, and HCOOH) from CO_2 through carbon fixation. Compared with the performance of commercial electrocatalysts, more research effort is still needed for the development of CTF-based electrocatalysts for the CO_2RR. Hopefully, continued study efforts in this burgeoning field will eventually lead to the large-scale application of EESC.

3.2.5 Multi-functional electrocatalysis. CTF-Based materials with excellent properties (*e.g.*, large SSA, suitable porosity, and copious active centers) have been regarded as high-performance multi-functional electrocatalysts for energy conversion. For example, Voort and co-workers designed a CTF-based material with variable N functionalities (pyridinic-N, triazine-N, quaternary-N, pyrrolic-N, and pyridine-N-oxide) as an efficient metal-free electrocatalyst for the ORR and HER.[205] The optimal sample exhibited an E_{onset} of 0.793 V and $E_{1/2}$ of 0.737 V *vs.* RHE in the ORR, together with remarkable HER performance of an overpotential of 0.31 V to achieve 10 mA cm^{-2} and small Tafel slope of 41 mV dec^{-1}. In another work, Janiak *et al.* deposited Pd and IrO_x nanoparticles on an N-rich CTF using an energy-saving microwave route to drive the reaction.[206] The developed samples demonstrated similar electrocatalytic behavior toward the HER and ORR in comparison to 20% commercial Pt/C.

Furthermore, Liu *et al.* prepared N-rich hollow carbon nanoflowers (N-HCNFs) from a preformed organic mesocrystal-CTF template by polymerization and subsequent carbonization.[207] The ideal hollow structure, sufficient N-doped active sites and large SSA led to efficient and durable bifunctional electrocatalytic activity for the ORR and HER. Consequently, an excellent electrochemical ORR performance with a positive $E_{1/2}$ of 0.84 V (*vs.* RHE), excellent stability, and methanol resistance were achieved in alkaline media. Additionally, great HER activity with a low overpotential of 243 mV at a current density of 10 mA cm^{-2} and small Tafel slope of 111 mV dec^{-1} in acidic media were demonstrated, as shown in Fig. 16.

Notably, Wu *et al.* developed a new approach to prepare N-doped carbon nanotubes from a newly designed CTF.[208] The rich N component, high conductivity, and optimum pyridinic-N content of the N-doped carbons led to superior and robust trifunctional electrocatalysts for the ORR, OER, and HER. This work demonstrated that well-defined CTFs can be converted into efficient and versatile electrocatalysts, providing a promising pathway to design multi-functional materials for EESC.

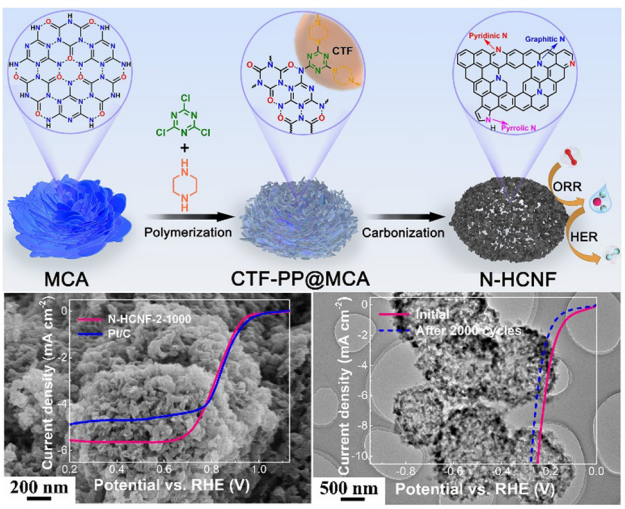

Fig. 16 Schematic illustration of the synthesis of N-HCNFs and the corresponding ORR/HER electrocatalytic performance. Reproduced from ref. 207 with permission from The Royal Society of Chemistry, Copyright 2020.

4. Conclusions and outlook

In this review, we summarized the recent advances in the development of CTF-based materials for EESC including supercapacitors, batteries, and electrocatalysis. Due to their unique structure, large SSA, and high content of N, CTFs have attracted significant research attention in the field of EESC. However, the practical application of CTFs is still limited owing to their poor conductivity induced by their high content of N. Thus, to extend the electrochemical application of CTFs, numerous studies on CTF-based hybrid materials and CTF-derived carbon materials have been conducted recently. By using CTFs as the precursors to synthesize CTF-based hybrid materials and CTF-derived carbon materials, the aptitudes of CTFs such as large SSA, controllable structures, large pore volumes, and tunable porosities can be inherited.

Despite the achievements by the research community in expanding the applications of CTFs, there are still several challenges that should not be neglected, as summarized below:

(1) For the preparation of CTFs, most of the synthesis methods are limited to the laboratory-scale owing to their tedious and complicated procedures. Hence, it is significant to develop simpler and more efficient procedures for the large-scale production of CTFs in industry. Besides, most of synthesis routes are generally toxic and risky. Therefore, the development of safe and green methods is an inevitable trend in the field of CTF-based material research and application. In addition, the applications of CTFs should be examined under industrial conditions to ensure their feasibility for real-life applications. More attention needs to be given to the scalability, sustainability, and economic potential of CTFs.

(2) The majority of CTFs that have been reported to date exhibit low crystallinity, which greatly limits their commercial application in industry. Thus, improving the crystallinity of CTFs and giving full play to their regular pore effect are still a hot research topic. Therefore, more research efforts should be devoted to improving the crystallinity of CTFs.

(3) The understanding of the structure and property relationships and the reaction mechanism is still largely lacking in this emerging field. Further research works on the precise engineering of active sites and advanced characterization techniques are needed to reveal the structure–performance relationship of CTFs for the development of highly efficient CTF-based nanomaterials.

(4) The electrochemical performance of CTF-based materials is still relatively low compared with most metal-based materials. Non-metal heteroatom doping such as N, S, P, and F is one of the most promising methods to improve the electrochemical performance of CTFs, resulting from the synergistic effects of defect formation and presence of foreign atoms. In addition, a high degree of graphitization can increase the conductivity and further enhance the electrochemical performance of CTF-based materials. However, the pore structures and carbon–heteroatom bonds in CTFs may be destroyed while being heated at relatively high temperatures. Hence, introducing foreign metals such as Mn, Ni, and Fe to achieve a higher degree of graphitization at relatively lower temperatures is a promising approach to prepare CTF-derived carbons with a high degree of graphitization. Therefore, we believe that the hybridization of metal-species with CTF-based carbon materials will lead to remarkable performances in the field of EESC.

(5) Further breakthroughs are needed for the synthesis of CTF materials with good intrinsic conductivity. Presently, most of the CTF materials reported exhibit semiconductor characteristics. To expand the application of CTFs in EESC, it is necessary to explore promising CTFs with good intrinsic conductivity. The synthesis of CTF materials with good intrinsic conductivity is beneficial for the directional control of the properties of these materials. Hence, the development of controllable chemical control means is necessary, and thus it is easier to realize the ''individual customization'' of these desirable materials.

(6) Given that structural features are a deciding factor in the electrochemical performance of EESC, the exploration of CTF-based nanomaterials with an ideal nanostructure and large SSA, tunable pore size, more abundant active sites, and better mass transfer is another important goal.

Although significant progress has been made in engineering molecular design in CTFs for EESC, there are still formidable limitations in yielding economically viable, high-performance materials. The further evolution of this area calls for the collaboration of scientists and engineers from different disciplines, both domestic and international. It is believed that CTF-related materials will have broader practical applications for EESC in the near future.

Conflicts of interest

There are no conflicts to declare.

Acknowledgements

We are grateful for the financial support from the National Natural Science Foundation of China (Grant No. 22006131 and 22276171), the Natural Science Foundation of Hubei Province (Grant No. 2022CFB820), and the Zhejiang Provincial Natural Science Foundation of China (Grant No. LQ20B070010).

Notes and references

1 X. Yang, C. Cheng, Y. Wang, L. Qiu and D. Li, *Science*, 2013, **341**, 534.
2 Y. Wang, Y. Song and Y. Xia, *Chem. Soc. Rev.*, 2016, **45**, 5925–5950.
3 L. Li, J. Meng, M. Zhang, T. Liu and C. Zhang, *Chem. Commun.*, 2022, **58**, 185–207.
4 T. Boruah, S. K. Das, G. Kumar, S. Mondal and R. S. Dey, *Chem. Commun.*, 2022, **58**, 5506–5509.
5 V. Etacheri, R. Marom, R. Elazari, G. Salitra and D. Aurbach, *Energy Environ. Sci.*, 2011, **4**, 3243–3262.
6 X. Cao, C. Tan, M. Sindoro and H. Zhang, *Chem. Soc. Rev.*, 2017, **46**, 2660–2677.
7 Y. He, X. Zhuang, C. Lei, L. Lei, Y. Hou, Y. Mai and X. Feng, *Nano Today*, 2019, **24**, 103–119.
8 P. Kuhn, M. Antonietti and A. Thomas, *Angew. Chem., Int. Ed.*, 2008, **47**, 3450–3453.

9 C. Reece, D. J. Willock and A. Trewin, *Phys. Chem. Chem. Phys.*, 2015, **17**, 817–823.
10 H. Ding, Y. Yang, B. Li, F. Pan, G. Zhu, M. Zeller, D. Yuan and C. Wang, *Chem. Commun.*, 2015, **51**, 1976–1979.
11 M. Ghashghaee, Z. Azizi and M. Ghambarian, *J. Phys. Chem. Solids*, 2020, **141**, 109422.
12 C. Krishnaraj, H. S. Jena, K. Leus and P. Van Der Voort, *Green Chem.*, 2020, **22**, 1038.
13 Y. Zheng, X. Ni, K. Li, X. Yu, H. Song, S. Chen, N. A. Khan, D. Wang and C. Zhang, *Compos. Commun.*, 2022, **32**, 101116–101122.
14 X. Wang, C. Zhang, Y. Zhao, S. Ren and J.-X. Jiang, *Macromol. Rapid Commun.*, 2016, **37**, 323.
15 S. Chen, Y. Zheng, B. Zhang, Y. Feng, J. Zhu, J. Xu, C. Zhang, W. Feng and T. Liu, *ACS Appl. Mater. Interfaces*, 2019, **11**, 1384–1393.
16 S. N. Talapaneni, T. H. Hwang, S. H. Je, O. Buyukcakir, J. W. Choi and A. Coskun, *Angew. Chem.*, 2016, **128**, 3158–3163.
17 L. Jiao, Y. Hu, H. Ju, C. Wang, M.-R. Gao, Q. Yang, J. Zhu, S.-H. Yu and H.-L. Jiang, *J. Mater. Chem. A*, 2017, **5**, 23170–23178.
18 Y. Zhu, X. Chen, J. Liu, J. Zhang, D. Xu, W. Peng, Y. Li, G. Zhang, F. Zhang and X. Fan, *ChemSusChem*, 2018, **11**, 2402–2409.
19 L. Tong, Z. Shao, Y. Qian and W. Li, *J. Mater. Chem. A*, 2017, **5**, 3832–3838.
20 F. Xu, D. Wu, R. Fu and B. Wei, *Mater. Today*, 2017, **20**, 629–656.
21 C. Zhu, H. Li, S. Fu, D. Du and Y. Lin, *Chem. Soc. Rev.*, 2016, **45**, 517–531.
22 Q. Lin, X. Bu, A. Kong, C. Mao, F. Bu and P. Feng, *Adv. Mater.*, 2015, **27**, 3431–3436.
23 L. Shao, S. Wang, M. Liu, J. Huang and Y.-N. Liu, *Chem. Eng. J.*, 2018, **339**, 509–518.
24 L. Shao, Y. Li, J. Huang and Y.-N. Liu, *Ind. Eng. Chem. Res.*, 2018, **57**, 2856–2865.
25 S. Dey, A. Bhunia, D. Esquivel and C. Janiak, *J. Mater. Chem. A*, 2016, **4**, 6259–6263.
26 A. K. Sekizkardes, S. Altarawneh, Z. Kahveci, T. İslamoğlu and H. M. El-Kaderi, *Macromolecules*, 2014, **47**, 8328–8334.
27 G. Xu, Y. Zhu, W. Xie, S. Zhang, C. Yao and Y. Xu, *Chem. – Asian J.*, 2019, **14**, 3259–3263.
28 C. Gu, D. Liu, W. Huang, J. Liu and R. Yang, *Polym. Chem.*, 2015, **6**, 7410–7417.
29 X. Chen, F. Yuan, Q. Gu and X. Yu, *J. Mater. Chem. A*, 2013, **1**, 11705–11710.
30 L. Shao, Y. Sang, J. Huang and Y.-N. Liu, *Chem. Eng. J.*, 2018, **353**, 1–14.
31 J. Guo, L. Wang and J. Huang, *Ind. Eng. Chem. Res.*, 2020, **59**, 3205–3212.
32 M. G. Mohamed, A. F. M. EL-Mahdy, M. M. M. Ahmed and S.-W. Kuo, *ChemPlusChem*, 2019, **84**, 1767–1774.
33 S. Mukherjee, M. Das, A. Manna, R. Krishna and S. Das, *Chem. Mater.*, 2019, **31**, 3929–3940.
34 Y. Fu, Z. Wang, S. Li, X. He, C. Pan, J. Yan and G. Yu, *ACS Appl. Mater. Interfaces*, 2018, **10**, 36002–36009.
35 H. Wang, D. Jiang, D. Huang, G. Zeng, P. Xu, C. Lai, M. Chen, M. Cheng, C. Zhang and Z. Wang, *J. Mater. Chem. A*, 2019, **7**, 22848–22870.
36 C. Krishnaraj, H. S. Jena, K. Leus and P. Van Der Voort, *Green Chem.*, 2020, **22**, 1038–1071.
37 J. Artz, *ChemCatChem*, 2018, **10**, 1753–1771.
38 R. Luo, W. Xu, M. Chen, X. Liu, Y. Fang and H. Ji, *ChemSusChem*, 2020, **13**, 6509–6522.
39 H. He, X. Chen, W. Zou and R. Li, *Int. J. Hydrogen Energy*, 2018, **43**, 2823–2830.
40 M. Liu, L. Guo, S. Jin and B. Tan, *J. Mater. Chem. A*, 2019, **7**, 5153–5172.
41 Y. Zhang and S. Jin, *Polymers*, 2019, **11**, 31.
42 N. Tahir, C. Krishnaraj, K. Leus and P. Van Der Voort, *Polymers*, 2019, **11**, 1326.
43 J. Xu, C. Zhu, S. Song, Q. Fang, J. Zhao and Y. Shen, *J. Hazard. Mater.*, 2022, **423**, 127004.
44 C. Zhu, Q. Fang, R. Liu, W. Dong, S. Song and Y. Shen, *Environ. Sci. Technol.*, 2022, **56**, 6699–6709.
45 P. Kuhn, A. Thomas and M. Antonietti, *Macromolecules*, 2009, **42**, 319–326.
46 P. Katekomol, J. Roeser, M. Bojdys, J. Weber and A. Thomas, *Chem. Mater.*, 2013, **25**, 1542–1548.
47 P. Kuhn, A. Forget, D. Su, A. Thomas and M. Antonietti, *J. Am. Chem. Soc.*, 2008, **130**, 13333–13337.
48 K. Wang, Y. Tang, Q. Jiang, Y. Lan, H. Huang, D. Liu and C. Zhong, *J. Energy Chem.*, 2017, **26**, 902–908.
49 J. Jia, Z. Chen, Y. Belmabkhout, K. Adil, P. M. Bhatt, V. A. Solovyeva, O. Shekhah and M. Eddaoudi, *J. Mater. Chem. A*, 2018, **6**, 15564–15568.
50 X. Cao, Q. Luo, F. Song, G. Liu, S. Chen, Y. Li, X. Li and Y. Lu, *Ind. Crops Prod.*, 2023, **191**, 115986.
51 W. Zhang, C. Li, Y.-P. Yuan, L.-G. Qiu, A.-J. Xie, Y.-H. Shen and J.-F. Zhu, *J. Mater. Chem.*, 2010, **20**, 6413–6415.
52 Z.-A. Lan, M. Wu, Z. Fang, Y. Zhang, X. Chen, G. Zhang and X. Wang, *Angew. Chem., Int. Ed.*, 2022, **61**, e202201482.
53 A. H. Cook and D. G. Jones, *J. Chem. Soc.*, 1941, 184–187, DOI: 10.1039/JR9410000184.
54 S. Ren, M. J. Bojdys, R. Dawson, A. Laybourn, Y. Z. Khimyak, D. J. Adams and A. I. Cooper, *Adv. Mater.*, 2012, **24**, 2357–2361.
55 X. Zhu, C. Tian, S. M. Mahurin, S.-H. Chai, C. Wang, S. Brown, G. M. Veith, H. Luo, H. Liu and S. Dai, *J. Am. Chem. Soc.*, 2012, **134**, 10478–10484.
56 S. Kuecken, J. Schmidt, L. Zhi and A. Thomas, *J. Mater. Chem. A*, 2015, **3**, 24422–24427.
57 H. Zhong, Z. Hong, C. Yang, L. Li, Y. Xu, X. Wang and R. Wang, *ChemSusChem*, 2019, **12**, 4493–4499.
58 Z. Li, Y. Han, Y. Guo, S. Xu, F. Chen, L. Ye, Z. Luo, X. Liu, H. Zhou and T. Zhao, *RSC Adv.*, 2017, **7**, 45818–45823.
59 J. Fan, X. Suo, T. Wang, Z. Wang, C.-L. Do-Thanh, S. M. Mahurin, T. Kobayashi, Z. Yang and S. Dai, *J. Mater. Chem. A*, 2022, **10**, 14310–14315.
60 T. Sun, Y. Liang, W. Luo, L. Zhang, X. Cao and Y. Xu, *Angew. Chem., Int. Ed.*, 2022, **61**, e202203327.
61 S.-Y. Yu, J. Mahmood, H.-J. Noh, J.-M. Seo, S.-M. Jung, S.-H. Shin, Y.-K. Im, I.-Y. Jeon and J.-B. Baek, *Angew. Chem., Int. Ed.*, 2018, **57**, 8438–8442.
62 S.-Y. Yu, J. C. Kim, H.-J. Noh, Y.-K. Im, J. Mahmood, I.-Y. Jeon, S. K. Kwak and J.-B. Baek, *Cell Rep. Phys. Sci.*, 2021, **2**, 100653.
63 F. Niu, Z.-W. Shao, L.-M. Tao and Y. Ding, *Sens. Actuators, B*, 2020, **321**, 128513.
64 K. Wang, L.-M. Yang, X. Wang, L. Guo, G. Cheng, C. Zhang, S. Jin, B. Tan and A. Cooper, *Angew. Chem., Int. Ed.*, 2017, **56**, 14149–14153.
65 M. Liu, Q. Huang, S. Wang, Z. Li, B. Li, S. Jin and B. Tan, *Angew. Chem., Int. Ed.*, 2018, **57**, 11968–11972.
66 Z. Qian, Z. J. Wang and K. A. I. Zhang, *Chem. Mater.*, 2021, **33**, 1909–1926.
67 P. Puthiaraj, S.-M. Cho, Y.-R. Lee and W.-S. Ahn, *J. Mater. Chem. A*, 2015, **3**, 6792–6797.
68 H. Lim, M. C. Cha and J. Y. Chang, *Macromol. Chem. Phys.*, 2012, **213**, 1385–1390.
69 P. Puthiaraj, S.-S. Kim and W.-S. Ahn, *Chem. Eng. J.*, 2016, **283**, 184–192.
70 T.-M. Geng, X.-C. Fang, F.-Q. Wang and F. Zhu, *Macromol. Mater. Eng.*, 2021, **306**, 2100461.
71 E. Troschke, S. Grätz, T. Lübken and L. Borchardt, *Angew. Chem., Int. Ed.*, 2017, **56**, 6859–6863.
72 Z. Xiang and D. Cao, *Macromol. Rapid Commun.*, 2012, **33**, 1184–1190.
73 S. Ren, R. Dawson, A. Laybourn, J.-X. Jiang, Y. Khimyak, D. J. Adams and A. I. Cooper, *Polym. Chem.*, 2012, **3**, 928–934.
74 T. Chen, W.-Q. Li, W.-B. Hu, W.-J. Hu, Y. A. Liu, H. Yang and K. Wen, *RSC Adv.*, 2019, **9**, 18008–18012.
75 H. R. Abuzeid, A. F. M. El-Mahdy, M. M. M. Ahmed and S.-W. Kuo, *Polym. Chem.*, 2019, **10**, 6010–6020.
76 C. Yang, W. Huang, L. C. da Silva, K. A. I. Zhang and X. Wang, *Chem. – Eur. J.*, 2018, **24**, 17454–17458.
77 C. Liao, Z. Liang, B. Liu, H. Chen, X. Wang and H. Li, *ACS Appl. Nano Mater.*, 2020, **3**, 2889–2898.
78 C. Krishnaraj, H. S. Jena, K. Leus, H. M. Freeman, L. G. Benning and P. Van Der Voort, *J. Mater. Chem. A*, 2019, **7**, 13188–13196.
79 Y. Zheng, S. Chen, H. Lu, C. Zhang and T. Liu, *Nanotechnology*, 2020, **31**, 364003–3644011.
80 H. Ding, A. Mal and C. Wang, *Chem. Res. Chin. Univ.*, 2022, **38**, 356–363.
81 M. Sajjad and W. Lu, *J. Energy Storage*, 2021, **39**, 102618.

82 J. Yan, Q. Wang, T. Wei and Z. Fan, *Adv. Energy Mater.*, 2014, **4**, 1300816.
83 D. Hulicova-Jurcakova, M. Kodama, S. Shiraishi, H. Hatori, Z. H. Zhu and G. Q. Lu, *Adv. Funct. Mater.*, 2009, **19**, 1800–1809.
84 L. L. Zhang and X. S. Zhao, *Chem. Soc. Rev.*, 2009, **38**, 2520–2531.
85 L. Hao, B. Luo, X. Li, M. Jin, Y. Fang, Z. Tang, Y. Jia, M. Liang, A. Thomas, J. Yang and L. Zhi, *Energy Environ. Sci.*, 2012, **5**, 9747–9751.
86 L. Hao, J. Ning, B. Luo, B. Wang, Y. Zhang, Z. Tang, J. Yang, A. Thomas and L. Zhi, *J. Am. Chem. Soc.*, 2015, **137**, 219–225.
87 Y. Li, S. Zheng, X. Liu, P. Li, L. Sun, R. Yang, S. Wang, Z.-S. Wu, X. Bao and W.-Q. Deng, *Angew. Chem., Int. Ed.*, 2018, **57**, 7992–7996.
88 L. Xu, R. Liu, F. Wang, S. Yan, X. Shi and J. Yang, *RSC Adv.*, 2019, **9**, 1586–1590.
89 M. G. Mohamed, A. F. M. El-Mahdy, Y. Takashi and S.-W. Kuo, *New J. Chem.*, 2020, **44**, 8241–8253.
90 A. F. M. El-Mahdy, C.-H. Kuo, A. Alshehri, C. Young, Y. Yamauchi, J. Kim and S.-W. Kuo, *J. Mater. Chem. A*, 2018, **6**, 19532–19541.
91 A. F. M. El-Mahdy, Y.-H. Hung, T. H. Mansoure, H.-H. Yu, T. Chen and S.-W. Kuo, *Chem. – Asian J.*, 2019, **14**, 1429–1435.
92 D. Liu, X.-a Ning, Y. Hong, Y. Li, Q. Bian and J. Zhang, *Electrochim. Acta*, 2019, **296**, 327–334.
93 L. Li, F. Lu, R. Xue, B. Ma, Q. Li, N. Wu, H. Liu, W. Yao, H. Guo and W. Yang, *ACS Appl. Mater. Interfaces*, 2019, **11**, 26355–26363.
94 P. Bhanja, K. Bhunia, S. K. Das, D. Pradhan, R. Kimura, Y. Hijikata, S. Irle and A. Bhaumik, *ChemSusChem*, 2017, **10**, 921–929.
95 E. Troschke, D. Leistenschneider, T. Rensch, S. Grätz, J. Maschita, S. Ehrling, B. Klemmed, B. V. Lotsch, A. Eychmüller, L. Borchardt and S. Kaskel, *ChemSusChem*, 2020, **13**, 3192–3198.
96 Y. Gao, C. Zhi, P. Cui, K. A. I. Zhang, L.-P. Lv and Y. Wang, *Chem. Eng. J.*, 2020, **400**, 125967.
97 M. Mahato, S. Nam, R. Tabassian, S. Oh, V. H. Nguyen and I.-K. Oh, *Adv. Funct. Mater.*, 2021, 2107442.
98 Y. Zhang, B. Zhang, L. Chen, T. Wang, M. Di, F. Jiang, X. Xu and S. Qiao, *J. Colloid Interface Sci.*, 2022, **606**, 1534–1542.
99 K. Yuan, T. Hu, Y. Xu, R. Graf, L. Shi, M. Forster, T. Pichler, T. Riedl, Y. Chen and U. Scherf, *Mater. Chem. Front.*, 2017, **1**, 278–285.
100 Y. Xu, S. Wu, S. Ren, J. Ji, Y. Yue and J. Shen, *RSC Adv.*, 2017, **7**, 32496–32501.
101 F. Hu, J. Wang, S. Hu, L. Li, W. Shao, J. Qiu, Z. Lei, W. Deng and X. Jian, *ACS Appl. Mater. Interfaces*, 2017, **9**, 31940–31949.
102 D.-G. Wang, H. Wang, Y. Lin, G. Yu, M. Song, W. Zhong and G.-C. Kuang, *ChemSusChem*, 2018, **11**, 3932–3940.
103 M. Kim, P. Puthiaraj, Y. Qian, Y. Kim, S. Jang, S. Hwang, E. Na, W.-S. Ahn and S. E. Shim, *Electrochim. Acta*, 2018, **284**, 98–107.
104 N. Deka, R. Patidar, S. Kasthuri, N. Venkatramaiah and G. K. Dutta, *Mater. Chem. Front.*, 2019, **3**, 680–689.
105 S. Vargheese, R. T. R. Kumar and Y. Haldorai, *Mater. Lett.*, 2019, **249**, 53–56.
106 L. Peng, Q. Guo, Z. Ai, Y. Zhao, Y. Liu and D. Wei, *Front. Chem.*, 2019, **7**, 142.
107 Y. Zhao, N. Bu, H. Shao, Q. Zhang, B. Feng, Y. Xu, G. Zheng, Y. Yuan, Z. Yan and L. Xia, *New J. Chem.*, 2019, **43**, 18158–18164.
108 M. M. Vadiyar, X. Liu and Z. Ye, *ACS Appl. Mater. Interfaces*, 2019, **11**, 45805–45817.
109 C. Wu, H. Zhang, M. Hu, G. Shan, J. Gao, J. Liu, X. Zhou and J. Yang, *Adv. Electron. Mater.*, 2020, **6**, 2000253.
110 D. Baumann, C. Lee, C. Wan, H. Sun and X. Duan, *ACS Mater. Lett.*, 2019, **1**, 320–326.
111 F. Hu, T. Zhang, J. Wang, S. Li, C. Liu, C. Song, W. Shao, S. Liu and X. Jian, *Nano Energy*, 2020, **74**, 104789.
112 Y. Gao, P. Cui, J. Liu, W. Sun, S. Chen, S. Chou, L.-P. Lv and Y. Wang, *ACS Appl. Energy Mater.*, 2021, **4**, 4519–4529.
113 J. Zhu, X. Zhuang, J. Yang, X. Feng and S.-I. Hirano, *J. Mater. Chem. A*, 2017, **5**, 16732–16739.
114 S. Yun, Y. Zhang, Q. Xu, J. Liu and Y. Qin, *Nano Energy*, 2019, **60**, 600–619.
115 X. Chen, H. Zhang, C. Ci, W. Sun and Y. Wang, *ACS Nano*, 2019, **13**, 3600–3607.
116 J. Yang, Z. Ju, Y. Jiang, Z. Xing, B. Xi, J. Feng and S. Xiong, *Adv. Mater.*, 2018, **30**, 1700104.
117 M. S. Whittingham, *Chem. Rev.*, 2004, **104**, 4271–4302.
118 K. Sakaushi, G. Nickerl, F. M. Wisser, D. Nishio-Hamane, E. Hosono, H. Zhou, S. Kaskel and J. Eckert, *Angew. Chem., Int. Ed.*, 2012, **51**, 7850–7854.
119 K. A. See, S. Hug, K. Schwinghammer, M. A. Lumley, Y. Zheng, J. M. Nolt, G. D. Stucky, F. Wudl, B. V. Lotsch and R. Seshadri, *Chem. Mater.*, 2015, **27**, 3821–3829.
120 H. Kang, H. Liu, C. Li, L. Sun, C. Zhang, H. Gao, J. Yin, B. Yang, Y. You, K.-C. Jiang, H. Long and S. Xin, *ACS Appl. Mater. Interfaces*, 2018, **10**, 37023–37030.
121 H. Zhang, W. Sun, X. Chen and Y. Wang, *ACS Nano*, 2019, **13**, 14252–14261.
122 Y. Zhu, X. Chen, Y. Cao, W. Peng, Y. Li, G. Zhang, F. Zhang and X. Fan, *Chem. Commun.*, 2019, **55**, 1434–1437.
123 O. Buyukcakir, J. Ryu, S. H. Joo, J. Kang, R. Yuksel, J. Lee, Y. Jiang, S. Choi, S. H. Lee, S. K. Kwak, S. Park and R. S. Ruoff, *Adv. Funct. Mater.*, 2020, **30**, 2003761.
124 Z. Wang, S. Gu, L. Cao, L. Kong, Z. Wang, N. Qin, M. Li, W. Luo, J. Chen, S. Wu, G. Liu, H. Yuan, Y. Bai, K. Zhang and Z. Lu, *ACS Appl. Mater. Interfaces*, 2021, **13**, 514–521.
125 C. Wu, M. Hu, X. Yan, G. Shan, J. Liu and J. Yang, *Energy Storage Mater.*, 2021, **36**, 347–354.
126 F. Jiang, Y. Wang, T. Qiu, Y. Zhang, W. Zhu, C. Yang, J. Huang, Z. Fang and G. Dai, *ACS Appl. Mater. Interfaces*, 2021, **13**, 48818–48827.
127 F. Jiang, Y. Wang, T. Qiu, G. Yang, C. Yang, J. Huang, Z. Fang and J. Li, *J. Power Sources*, 2022, **523**, 231041.
128 B. Ball, C. Chakravarty and P. Sarkar, *J. Phys. Chem. C*, 2019, **123**, 30155–30164.
129 R. Yuan, W. Kang and C. Zhang, *Materials*, 2018, **11**, 937.
130 J. Zhu, J. Yang, Z. Xu, J. Wang, Y. Nuli, X. Zhuang and X. Feng, *Nanoscale*, 2017, **9**, 8871–8878.
131 X. Gao, X. Zhang, J. Jiang and J. Chen, *Mater. Lett.*, 2018, **228**, 42–45.
132 K. Sakaushi, E. Hosono, G. Nickerl, T. Gemming, H. Zhou, S. Kaskel and J. Eckert, *Nat. Commun.*, 2013, **4**, 1485.
133 J. Liu, P. Lyu, Y. Zhang, P. Nachtigall and Y. Xu, *Adv. Mater.*, 2018, **30**, 1705401.
134 N. Yang, Y. Gu, Y. Shan, C. Tian, L. Yang, H. Jiang, H. Liu, X. Zhu and S. Dai, *ACS Macro Lett.*, 2022, **11**, 60–65.
135 S.-Y. Li, W.-H. Li, X.-L. Wu, Y. Tian, J. Yue and G. Zhu, *Chem. Sci.*, 2019, **10**, 7695–7701.
136 R. Meng, Q. Deng, C. Peng, B. Chen, K. Liao, L. Li, Z. Yang, D. Yang, L. Zheng, C. Zhang and J. Yang, *Nano Today*, 2020, **35**, 100991.
137 Y.-X. Yin, S. Xin, Y.-G. Guo and L.-J. Wan, *Angew. Chem., Int. Ed.*, 2013, **52**, 13186–13200.
138 R. D. Rauh, K. M. Abraham, G. F. Pearson, J. K. Surprenant and S. B. Brummer, *J. Electrochem. Soc.*, 1979, **126**, 523.
139 H. Liao, H. Ding, B. Li, X. Ai and C. Wang, *J. Mater. Chem. A*, 2014, **2**, 8854–8858.
140 S. H. Je, H. J. Kim, J. Kim, J. W. Choi and A. Coskun, *Adv. Funct. Mater.*, 2017, **27**, 1703947.
141 F. Xu, S. Yang, G. Jiang, Q. Ye, B. Wei and H. Wang, *ACS Appl. Mater. Interfaces*, 2017, **9**, 37731–37738.
142 S. Yang, Q. Liu, Q. Lu, E. Zhang, U. S. Arrozi, H. Li, S. Kaskel, F. Xu and H. Wang, *Energy Technol.*, 2019, **7**, 1900583.
143 D.-G. Wang, L. Tan, H. Wang, M. Song, J. Wang and G.-C. Kuang, *ChemElectroChem*, 2019, **6**, 2777–2781.
144 E. Troschke, C. Kensy, F. Haase, S. Dörfler, Y. Joseph, B. V. Lotsch and S. Kaskel, *Batteries Supercaps*, 2020, **3**, 1069–1079.
145 T. Zhang, F. Hu, C. Song, S. Li, W. Shao, S. Liu, H. Peng, S. Hu and X. Jian, *Chem. Eng. J.*, 2021, **407**, 127141.
146 G. Gao, Y. Jia, H. Gao, W. Shi, J. Yu, Z. Yang, Z. Dong and Y. Zhao, *ACS Appl. Mater. Interfaces*, 2021, **13**, 50258–50269.
147 R. Guan, L. Zhong, S. Wang, D. Han, M. Xiao, L. Sun and Y. Meng, *ACS Appl. Mater. Interfaces*, 2020, **12**, 8296–8305.
148 J. Kim, A. Elabd, S.-Y. Chung, A. Coskun and J. W. Choi, *Chem. Mater.*, 2020, **32**, 4185–4193.
149 Q. X. Shi, H. J. Pei, N. You, J. Wu, X. Xiang, Q. Xia, X. L. Xie, S. B. Jin and Y. S. Ye, *Chem. Eng. J.*, 2019, **375**, 121977.
150 Q. X. Shi, C. Y. Yang, H. J. Pei, C. Chang, X. Guan, F. Y. Chen, X. L. Xie and Y. S. Ye, *Chem. Eng. J.*, 2021, **404**, 127044.
151 S. Ni, Z. Li and J. Yang, *Nanoscale*, 2012, **4**, 1184–1189.
152 Z. Xiang, D. Cao, L. Huang, J. Shui, M. Wang and L. Dai, *Adv. Mater.*, 2014, **26**, 3315–3320.
153 J. Liu, Y. Hu and J. Cao, *Catal. Commun.*, 2015, **66**, 91–94.
154 W. Yu, S. Gu, Y. Fu, S. Xiong, C. Pan, Y. Liu and G. Yu, *J. Catal.*, 2018, **362**, 1–9.

155 T. Sönmez, K. S. Belthle, A. Iemhoff, J. Uecker, J. Artz, T. Bisswanger, C. Stampfer, H. H. Hamzah, S. A. Nicolae, M.-M. Titirici and R. Palkovits, *Catal. Sci. Technol.*, 2021, **11**, 6191–6204.
156 L.-Z. Peng, P. Liu, Q.-Q. Cheng, W.-J. Hu, Y. A. Liu, J.-S. Li, B. Jiang, X.-S. Jia, H. Yang and K. Wen, *Chem. Commun.*, 2018, **54**, 4433–4436.
157 K. Kamiya, R. Kamai, K. Hashimoto and S. Nakanishi, *Nat. Commun.*, 2014, **5**, 5040.
158 K. Iwase, T. Yoshioka, S. Nakanishi, K. Hashimoto and K. Kamiya, *Angew. Chem., Int. Ed.*, 2015, **54**, 11068–11072.
159 K. Iwase, K. Kamiya, M. Miyayama, K. Hashimoto and S. Nakanishi, *ChemElectroChem*, 2018, **5**, 805–810.
160 J.-D. Yi, R. Xu, Q. Wu, T. Zhang, K.-T. Zang, J. Luo, Y.-L. Liang, Y.-B. Huang and R. Cao, *ACS Energy Lett.*, 2018, **3**, 883–889.
161 S. Zhou, Z. Xiao, Q. Yang, X. Huang, Y. Niu, Y. Ma and L. Zhi, *Sci. China: Mater.*, 2021, **64**, 2221–2229.
162 S. Chen, Y. Zhu, D. Xu, W. Peng, Y. Li, G. Zhang, F. Zhang and X. Fan, *ChemElectroChem*, 2018, **5**, 717–721.
163 M. Yang, Y. Liu, H. Chen, D. Yang and H. Li, *ACS Appl. Mater. Interfaces*, 2016, **8**, 28615–28623.
164 Y. Cao, Y. Zhu, X. Chen, B. S. Abraha, W. Peng, Y. Li, G. Zhang, F. Zhang and X. Fan, *Catal. Sci. Technol.*, 2019, **9**, 6606–6612.
165 Y. Zheng, S. Chen, K. A. I. Zhang, J. Guan, X. Yu, W. Peng, H. Song, J. Zhu, J. Xu, X. Fan, C. Zhang and T. Liu, *J. Colloid Interface Sci.*, 2022, **608**, 3168–3177.
166 N. Li, R. Tang, Y. Su, C. Lu, Z. Chen, J. Sun, Y. Lv, S. Han, C. Yang and X. Zhuang, *ChemSusChem*, 2023, e202201937.
167 K. Jiang, P. Peng, D. Tranca, G. Tong, C. Ke, C. Lu, J. Hu, H. Liang, J. Li, S. Zhou, E. Kymakis and X. Zhuang, *Macromol. Rapid Commun.*, 2022, **43**, 2200392.
168 Y. Zheng, H. Song, S. Chen, X. Yu, J. Zhu, J. Xu, K. A. I. Zhang, C. Zhang and T. Liu, *Small*, 2020, **16**, 2004342–2004352.
169 Y. Zheng, S. Chen, K. A. I. Zhang, J. Zhu, J. Xu, C. Zhang and T. Liu, *ACS Appl. Mater. Interfaces*, 2021, **13**, 13328–13337.
170 C. Chen, H. Han, X. Liu, Y. Chen, D. Wu, Z. Gao, S. Gao and K. Jiang, *Microporous Mesoporous Mater.*, 2021, **325**, 111335.
171 Q. Zuo, P. Zhao, W. Luo and G. Cheng, *Nanoscale*, 2016, **8**, 14271–14277.
172 R. Dun, M. Hao, Y. Su and W. Li, *J. Mater. Chem. A*, 2019, **7**, 12518–12525.
173 R. Dun, M. Hao, Y. Su and W. Li, *ACS Appl. Mater. Interfaces*, 2021, **13**, 52479–52486.
174 S. Zhang, X. Liu, Z. Li, L. Hao, P. Wang, X. Zou, Z. Liu, G. Zhang and C.-Y. Zhang, *ACS Sustainable Chem. Eng.*, 2019, **7**, 11787–11794.
175 S. Wei, F. Zhang, Z. Chen, J. Ding, B. Xue and C. Lu, *New J. Chem.*, 2020, **44**, 12850–12856.
176 Y. Dong, L. Gu, C. Wang, Y. Du, W. Bo, H. Du, Y. Wang and J. Zhao, *J. Electroanal. Chem.*, 2022, **924**, 116879.
177 M. Lv, C. Luo, J. Li, Y. Zhang, Q. Zeng, N. Huang, S. Wang, Y. Zheng, W. Liu and L. Ye, *ACS Mater. Lett.*, 2023, **5**, 744–752.
178 S. Xiong, M. Lin, L. Wang, S. Liu, S. Weng, S. Jiang, Y. Xu, Y. Jiao and J. Chen, *Appl. Surf. Sci.*, 2021, **546**, 149064.
179 S. Gopi and M. Kathiresan, *Polymer*, 2017, **109**, 315–320.
180 S. Öztürk, Y.-X. Xiao, D. Dietrich, B. Giesen, J. Barthel, J. Ying, X.-Y. Yang and C. Janiak, *Beilstein J. Nanotechnol.*, 2020, **11**, 770–781.
181 X. Gao, Y.-J. Gao, S.-Q. Li, J. Yang, G.-L. Zhuang, S.-W. Deng, Z.-H. Yao, X. Zhong, Z.-Z. Wei and J.-G. Wang, *J. Energy Chem.*, 2020, **50**, 135–142.
182 H.-F. Wang, L. Chen, H. Pang, S. Kaskel and Q. Xu, *Chem. Soc. Rev.*, 2020, **49**, 1414–1448.
183 S. Gopi, K. Giribabu and M. Kathiresan, *ACS Omega*, 2018, **3**, 6251–6258.
184 Y. Hua, X. Li, C. Chen and H. Pang, *Chem. Eng. J.*, 2019, **370**, 37–59.
185 J.-S. Li, Y.-J. Tang, C.-H. Liu, S.-L. Li, R.-H. Li, L.-Z. Dong, Z.-H. Dai, J.-C. Bao and Y.-Q. Lan, *J. Mater. Chem. A*, 2016, **4**, 1202–1207.
186 B. Ball, C. Chakravarty and P. Sarkar, *J. Phys. Chem. Lett.*, 2020, **11**, 1542–1549.
187 J.-D. Yi, R. Xu, G.-L. Chai, T. Zhang, K. Zang, B. Nan, H. Lin, Y.-L. Liang, J. Lv, J. Luo, R. Si, Y.-B. Huang and R. Cao, *J. Mater. Chem. A*, 2019, **7**, 1252–1259.
188 Z. Li, J. Zhang, X. Jing, J. Dong, H. Liu, H. Lv, Y. Chi and C. Hu, *J. Mater. Chem. A*, 2021, **9**, 6152–6159.
189 B. Zhang, Y. Zhang, M. Hou, W. Wang, S. Hu, W. Cen, X. Cao, S. Qiao and B.-H. Han, *J. Mater. Chem. A*, 2021, **9**, 10146–10159.
190 S. Qiao, B. Zhang, Q. Li, Z. Li, W. Wang, J. Zhao, X. Zhang and Y. Hu, *ChemSusChem*, 2019, **12**, 5032–5040.
191 C. Hu, Y. Xiao, Y. Zou and L. Dai, *Electrochem. Energy Rev.*, 2018, **1**, 84–112.
192 K. P. Kuhl, T. Hatsukade, E. R. Cave, D. N. Abram, J. Kibsgaard and T. F. Jaramillo, *J. Am. Chem. Soc.*, 2014, **136**, 14107–14113.
193 X. Zhu, C. Tian, H. Wu, Y. He, L. He, H. Wang, X. Zhuang, H. Liu, C. Xia and S. Dai, *ACS Appl. Mater. Interfaces*, 2018, **10**, 43588–43594.
194 Y. Wang, J. Chen, G. Wang, Y. Li and Z. Wen, *Angew. Chem., Int. Ed.*, 2018, **57**, 13120–13124.
195 J. Yi, Q. Li, S. Chi, Y. Huang and R. Cao, *Chem. Res. Chin. Univ.*, 2022, **38**, 141–146.
196 A. Laemont, S. Abednatanzi, P. G. Derakshandeh, F. Verbruggen, E. Fiset, Q. Qin, K. Van Daele, M. Meledina, J. Schmidt, M. Oschatz, P. Van Der Voort, K. Rabaey, M. Antonietti, T. Breugelmans and K. Leus, *Green Chem.*, 2020, **22**, 3095.
197 S. Kato, T. Hashimoto, K. Iwase, T. Harada, S. Nakanishi and K. Kamiya, *Chem. Sci.*, 2023, **14**, 613–620.
198 L. Gong, X. Wang, T. Zheng, J. Liu, J. Wang, Y.-C. Yang, J. Zhang, X. Han, L. Zhang and Z. Xia, *J. Mater. Chem. A*, 2021, **9**, 3555–3566.
199 P. Su, K. Iwase, T. Harada, K. Kamiya and S. Nakanishi, *Chem. Sci.*, 2018, **9**, 3941–3947.
200 S. Feng, W. Zheng, J. Zhu, Z. Li, B. Yang, Z. Wen, J. Lu, L. Lei, S. Wang and Y. Hou, *Appl. Catal., B*, 2020, **270**, 118908.
201 C. Lu, J. Yang, S. Wei, S. Bi, Y. Xia, M. Chen, Y. Hou, M. Qiu, C. Yuan, Y. Su, F. Zhang, H. Liang and X. Zhuang, *Adv. Funct. Mater.*, 2019, **29**, 1806884.
202 N. Yang, L. Yang, X. Zhu, P. Zhao, H. Liu, C. Xia, S. Dai and C. Tian, *ACS Mater. Lett.*, 2022, **4**, 2143–2150.
203 L. Ma, W. Hu, B. Mei, H. Liu, B. Yuan, J. Zang, T. Chen, L. Zou, Z. Zou, B. Yang, Y. Yu, J. Ma, Z. Jiang, K. Wen and H. Yang, *ACS Catal.*, 2020, **10**, 4534–4542.
204 M.-J. Mao, M.-D. Zhang, D.-L. Meng, J.-X. Chen, C. He, Y.-B. Huang and R. Cao, *ChemCatChem*, 2020, **12**, 3530–3536.
205 H. S. Jena, C. Krishnaraj, S. Parwaiz, F. Lecoeuvre, J. Schmidt, D. Pradhan and P. Van Der Voort, *ACS Appl. Mater. Interfaces*, 2020, **12**, 44689–44699.
206 L. Rademacher, T. H. Y. Beglau, T. Heinen, J. Barthel and C. Janiak, *Front. Chem.*, 2022, **10**, 945261.
207 Y. Zheng, S. Chen, H. Song, H. Guo, K. A. I. Zhang, C. Zhang and T. Liu, *Nanoscale*, 2020, **12**, 14441–14447.
208 J. Zeng, Z. Chen, X. Zhao, W. Yu, S. Wu, J. Lu, K. P. Loh and J. Wu, *ACS Appl. Nano Mater.*, 2019, **2**, 7969–7977.
209 Y. Su, Y. Liu, P. Liu, D. Wu, X. Zhuang, F. Zhang and X. Feng, *Angew. Chem., Int. Ed.*, 2015, **54**, 1812–1816.
210 Z. Lei, X. Chen, W. Sun, Y. Zhang and Y. Wang, *Adv. Energy Mater.*, 2019, **9**, 1801010.
211 K. Sakaushi, E. Hosono, G. Nickerl, H. Zhou, S. Kaskel and J. Eckert, *J. Power Sources*, 2014, **245**, 553–556.
212 T. Kesavan, T. Partheeban, M. Vivekanantha, N. Prabu, M. Kundu, P. Selvarajan, S. Umapathy, A. Vinu and M. Sasidharan, *ACS Appl. Mater. Interfaces*, 2020, **12**, 24007–24018.
213 S.-B. Ren, W. Ma, C. Zhang, L. Chen, K. Wang, R.-R. Li, M. Shen, D.-M. Han, Y. Chen and J.-X. Jiang, *ChemSusChem*, 2020, **13**, 2295–2302.
214 S. Wang, Q. Wang, P. Shao, Y. Han, X. Gao, L. Ma, S. Yuan, X. Ma, J. Zhou, X. Feng and B. Wang, *J. Am. Chem. Soc.*, 2017, **139**, 4258–4261.
215 J. Xu, F. Yu, J. Hua, W. Tang, C. Yang, S. Hu, S. Zhao, X. Zhang, Z. Xin and D. Niu, *Chem. Eng. J.*, 2020, **392**, 123694.
216 D.-G. Wang, Y. Wang, M. Song, G.-C. Kuang and K. Han, *Chem. Commun.*, 2019, **55**, 13247–13250.
217 X. Liu, S. Wang, A. Wang, J. Chen, Z. Wang, Q. Zeng, W. Liu, Z. Li and L. Zhang, *J. Phys. Chem. C*, 2019, **123**, 21327–21335.
218 Z. Yang, C. Peng, R. Meng, L. Zu, Y. Feng, B. Chen, Y. Mi, C. Zhang and J. Yang, *ACS Cent. Sci.*, 2019, **5**, 1876–1883.
219 L. Hao, S. Zhang, R. Liu, J. Ning, G. Zhang and L. Zhi, *Adv. Mater.*, 2015, **27**, 3189.